Scaling laws for Bénard-Marangoni convection at infinite Prandtl number

Author: Anton Pershin
Supervisor: Dr. Andrew Wynn

Department of Aeronautics
Imperial College London
South Kensington Campus
London, UK

September 9, 2016

Acknowledgements

First and foremost, I would like to thank sincerely my supervisor, Dr. Andrew Wynn, who has given me an opportunity to dive into the exciting research by his undoubtedly wise guidance. The questions that he has often raised during our meetings encouraged me to think and investigate the problem in various directions.

I would also like to thank Giovanni Fantuzzi who has actively participated in my project and his contribution into both numerical and analytical parts of the project is gratefully acknowledged.

I owe my sincere gratitude to my family for their advice and care during the whole year.

Finally, I am thankful to Victoria who has supported me throughout the studies in London. Without you this thesis would have not been possible.

Abstract

The present work regards the scaling laws for a vertical heat transport quantified by Nusselt number with respect to Marangoni number in the context of Bénard-Marangoni convection at infinite Prandtl number.

The optimal scaling law for an upper bound on Nusselt number is obtained by applying semidefinite programming to the variational optimization problem formulated by Hagstrom and Doering in [9]. The leading role of the right boundary layer of the background temperature profile in improvement of the scaling law is demonstrated by a sequence of numerical experiments.

The self-similar parametrized background profile and its application to the variational problem stated by Hagstrom and Doering are investigated analytically for the case when the right boundary layer is set by the positive constant function. The possible improvements of the parametrized background profile taking into account the features of the fully optimal background profile are proposed.

Table of Contents

Introduction

In 1900, Henri Bénard, a French physicist, discovered a cellular pattern in a layer of fluid heated from below. At every cell he observed an upward flow in its centre and a downward flow on the outer surface. It was understood later in a theoretical way [1] that this pattern can be produced by buoyancy, a force appearing in fluids due to a density gradient and gravity. The fluid becomes less dense at the heated lower surface causing thus a density gradient that results in a force acting upward. This force triggers a motion of the fluid which surprisingly leads to a self-organizing stable cellular pattern. Such a type of convection is now known as Rayleigh-Bénard convection. A particular configuration of the flow depends on Rayleigh number (Ra) that defines the ratio of gravitational forces to viscous forces. As buoyancy in Rayleigh-Bénard convection depends on the temperature difference between two side of a layer of fluid, Rayleigh number grows as the temperature difference increases. Then, the following flow states can be observed depending on the temperature difference [2]:

- $0 < \mathrm{Ra} \lesssim 1700$: linear temperature gradient with no motion (thermal conductivity);
- $1700 \lesssim \mathrm{Ra} \lesssim \mathcal{O}(10^6)$: rotating Bénard cells triggered by buoyancy (thermal convection);
- $\mathrm{Ra} \gtrsim \mathcal{O}(10^6)$: turbulent convection.

Rayleigh number at which Bénard cells and thermal convection appear ($\mathrm{Ra} \approx 1700$) is referred to as a critical Rayleigh number. One can note that at Ra more than 10^3 times the critical Rayleigh number Bénard cells no longer exist and the flow becomes turbulent.

However, the buoyancy effect is not the only physical mechanism allowing Bénard cells to exist. The second one is known as Marangoni effect, that is a motion of fluid due to a surface tension gradient. The most famous example of Marangoni effect is "tears of wine" which can be observed at a wineglass' surface where there is often a layer of liquid with an alcohol concentration gradient: it is higher near the surface of wine and becomes lower in the upward direction. Since pure water has a much stronger surface tension compared to alcohol's one, an upper layer of water appearing due to evaporation of alcohol attracts the fluid from below which returns back because of its own weight in the form of "tears". In this case, the surface tension gradient occurs due to the concentration gradient, but it can be also produced by a temperature difference. As a surface tension usually increases as a temperature decreases, we can conclude that if a temperature is not uniform at some free surface, then a surface tension gradient will appear on it. It was shown experimentally [3] and theoretically [4] that, for a thin layer of fluid heated from below and cooled from above with a free upper surface, the surface tension gradient occurring on it can indeed cause Bénard cells. This type of convection is known as Bénard-Marangoni convection.

It is interesting to note that Henri Bénard proposed in his original work that a surface tension may be related to the presence of cells because the upper surface of a layer of fluid was clearly deformed in his

experiment, but he decided to attribute it to buoyancy. However, as argued in [5], his experiment in fact was an example of Marangoni effect as there was a thin layer of fluid with a free upper surface.

Nowadays, surface-tension-driven convection has been found to play a leading role in numerous engineering application. For example, Marangoni effect appeared to be significant in melting [6] and crystal growth in semiconductors [7]. Schatz and Neitzel in [7] mention that Bénard-Marangoni convection is especially significant for layers of small sizes and also in the presence of microgravity because in both cases a buoyancy effect may be negligible. Not surprisingly that a great deal of examples can be found in the cases where a drying process of a thin film of liquid takes place: for instance, a drying polymer film [8].

Non-dimensional controller of Bénard-Marangoni convection is Marangoni number which essentially defines the ratio of surface tension forces to viscous forces. Since a surface tension depends on a temperature, then Marangoni number is expected to depend on $d\tau/dT$ where τ is surface tension. In other words, the higher Marangoni number, the more sensitive surface tension gradient to slight changes in temperature.

It is important to note, that unlike Rayleigh-Bénard convection Bénard-Marangoni convection does not necessarily become turbulent. This appeared to be determined by Prandtl number, i.e. the ratio of kinematic viscosity to thermal diffusivity. It was shown by numerical simulations of Bénard-Marangoni convection [10] that for high Prandtl numbers ($\mathrm{Pr} \approx 100$) the transition to turbulent regime does not occur even for very large Marangoni numbers (10^4 times critical Marangoni number at which Bénard cells and thermal convection appear).

Another important fact obtained from the numerical simulations [10] is that the numerical results for high Prandtl numbers almost exactly coincide with numerical results for infinite Prandtl number for chosen Marangoni numbers. Therefore, it is of prime interest to analyse Bénard-Marangoni convection at $\mathrm{Pr} = \infty$. The flow's configuration basing on Marangoni number at $\mathrm{Pr} = \infty$ is as follows [9]:

- $0 < \mathrm{Ma} \lesssim 60$: linear temperature gradient with no motion (thermal conductivity);
- $\mathrm{Ma} \gtrsim 60$: Bénard cells and thermal convection.

The present work is fully devoted to the case of infinite Prandtl number.

When a layer of fluid subjected to heating from below and cooling from above is considered in engineering applications, it is usually necessary to quantify a heat transfer between two sides of the layer. It can be done by using Nusselt number which is an inverse of the temperature difference between lower and upper surfaces:

$$\mathrm{Nu} = \frac{1}{T_{bottom} - T_{top}}. \tag{1.1}$$

It is easy to see that if the temperature difference tends to zero which corresponds to a perfect heat transfer, Nusselt number approaches infinity. In other words, the larger Nusselt number corresponds to the better vertical heat transport. In experiments and numerical simulations Nusselt number is usually calculated by taking space-time averages of temperatures on both surfaces. Boeck and Thess in [10] concluded from numerical simulations at infinite Prandtl number that Nusselt number starts obeying a power law with respect to Marangoni number when $\mathrm{Ma} \gtrsim 10^4$:

$$\mathrm{Nu} = 0.446\mathrm{Ma}^{0.238} \approx 0.446\mathrm{Ma}^{5/21}. \tag{1.2}$$

The first theoretical attempt to derive a scaling law for Nusselt number was made by Pumir and Blumenfled in [11] where the following phenomenological scaling law was suggested for large Prandtl number

$$\mathrm{Nu} \propto \mathrm{Ma}^{1/3}\mathrm{Pr}^{1/3}. \tag{1.3}$$

The most recent result regarding scaling laws of Nusselt number in Bénard-Marangoni convection is provided by Hagstrom and Doering in [9]. They made use of the background flow method to obtain a rigorous upper bound on Nusselt number. The background flow method suggested by Doering and Constantin in [12] is based on the idea that variational statements for upper and lower bounds of necessary quantities in the flows governed by PDEs may be derived if a flow is decomposed into two parts: a time-independent background profile absorbing all boundary conditions of the full flow and a fluctuating time-dependent remainder equipped with homogeneous boundary conditions. Since there is not any assumption about flow fields here, this technique allows us to construct variational bounds for a general case without being restricted by only laminar or turbulent flows. The background profile method has been already successfully applied to boundary-driven shear flows [13], Boussinesq equations [14], Rayleigh-Benard convection [15, 16] and recently to Bénard-Marangoni convection [9] and has allowed to derive new rigorous bounds on energy dissipation and heat transport.

By applying this technique to a simple Pearson's model that will be discussed in the next section, they formulated a variational optimization problem for Nusselt number and then derived a mathematically rigorous upper bound on Nusselt number at infinite Prandtl number

$$\mathrm{Nu} < 0.838\mathrm{Ma}^{2/7} = 0.838\mathrm{Ma}^{0.286}. \tag{1.4}$$

It is easy to see that the exponent in the power law (1.2) obtained from numerical simulations is 16.7% lower compared to (1.4). In this work we aim to improve the rigorous upper bound on Nusselt number by further numerical and analytical investigation of the variational optimization problem suggested by Hagstrom and Doering.

1.1 Pearson's model

One of the models describing Marangoni phenomenon is called Pearson's model which was historically the first model allowing an appearance of Bénard cells due to surface tension gradient [4]. This model describes Bénard-Marangoni convection for a simple geometry with a fixed lower surface and a nondeformable upper surface at which constant temperature and constant negative temperature flux are set respectively and a heat flux imposed through the layer. The two-dimensional statement of this model as presented in [9] is

$$\frac{1}{\mathrm{Pr}}\left(\frac{\partial \boldsymbol{u}}{\partial t} + \boldsymbol{u}\cdot\nabla\boldsymbol{u}\right) = -\nabla p + \nabla^2\boldsymbol{u}, \tag{1.5}$$

$$\nabla\cdot\boldsymbol{u} = 0, \tag{1.6}$$

$$\frac{\partial T}{\partial t} + \boldsymbol{u}\cdot\nabla T = \nabla^2 T, \tag{1.7}$$

where $\boldsymbol{u} := \boldsymbol{i}u(\boldsymbol{x},t) + \boldsymbol{k}w(\boldsymbol{x},t)$ is a vector velocity field, $p(\boldsymbol{x},t)$ is a scalar pressure field and $T(\boldsymbol{x},t)$ is a scalar temperature field. These equations are equipped with boundary conditions setting the fixed bottom

surface of the layer with constant temperature and no-slip:

$$u|_{z=0} = 0,\ w|_{z=0} = 0, \tag{1.8}$$

$$T|_{z=0} = 0. \tag{1.9}$$

The negative temperature flux has to be set on the top surface in order to model cooling. Together with an assumption that the upper surface of the layer does not deform, the resulting boundary conditions are

$$w|_{z=1} = 0, \tag{1.10}$$

$$\frac{\partial T}{\partial z}|_{z=1} = -1, \tag{1.11}$$

$$\left[\frac{\partial u}{\partial z} + \mathrm{Ma}\frac{\partial T}{\partial x}\right]_{z=1} = 0, \tag{1.12}$$

where $Ma := \gamma q h^2/\lambda\rho\nu\kappa$ in which γ is a negative derivative of surface tension with respect to T, q is an imposed heat and other quantities determine thermal, viscous and dense properties of the fluid. Note that unlike Rayleigh number in models for Rayleigh-Bénard convection where Ra is present in thermal conduction equation [2], Marangoni number is included into the boundary condition for the upper surface.

Finally, periodic boundary conditions are imposed in the horizontal direction corresponding to the x-coordinate on temperature, pressure and velocity fields, that is

$$\boldsymbol{u}|_{z=0} = \boldsymbol{u}|_{z=2\pi},\ T|_{z=0} = T|_{z=2\pi},\ p|_{z=0} = p|_{z=2\pi}. \tag{1.13}$$

In the limit $\mathrm{Pr} = \infty$, momentum (1.5) reduces to

$$\nabla p = \nabla^2 \boldsymbol{u} \tag{1.14}$$

and taking the divergence and applying the incompressibility condition (1.6) we can obtain $\nabla^2 p = 0$ implying that p is harmonic. Similarly, taking ∇^2 of both sides of (1.14) gives $\nabla^4 \boldsymbol{u} = 0$ which, in turn, implies that every component of $\boldsymbol{u}$ is biharmonic.

The periodic boundary conditions (1.13) allow us to expand u, v, w, T into Fourier series

$$u(\boldsymbol{x}, t) = \sum_{k=-\infty}^{+\infty} \hat{u}_k(z, t) e^{ikx}, \tag{1.15}$$

$$v(\boldsymbol{x}, t) = \sum_{k=-\infty}^{+\infty} \hat{v}_k(z, t) e^{ikx}, \tag{1.16}$$

$$w(\boldsymbol{x}, t) = \sum_{k=-\infty}^{+\infty} \hat{w}_k(z, t) e^{ikx}, \tag{1.17}$$

$$T(\boldsymbol{x}, t) = \sum_{k=-\infty}^{+\infty} \hat{T}_k(z, t) e^{ikx}. \tag{1.18}$$

Now consider the solution only for w since it will be of interest in the next section. The biharmonic equation for w then can be written

$$\sum_{k=-\infty}^{+\infty} \nabla^2\nabla^2 \left(\hat{w}_k e^{ikx}\right) = 0. \tag{1.19}$$

Therefore, the following equation must be satisfied for every Fourier mode and at every instant of time:

$$\frac{\partial^4 \hat{w}_k}{\partial z^4} - 2k^2 \frac{\partial^2 \hat{w}_k}{\partial z^2} + k^4 \hat{w}_k = 0. \tag{1.20}$$

The first two boundary conditions come directly from (1.8) and (1.10): $\hat{w}_k|_{z=0} = 0, \hat{w}_k|_{z=1} = 0$. Two other boundary conditions necessary for the fourth-order differential equation are derived from (1.12) and the incompressibility condition. Namely, (1.6) in terms of Fourier coefficients is

$$ik\hat{u}_k + \frac{\partial \hat{w}_k}{\partial z} = 0 \tag{1.21}$$

which substituting $\hat{u}_k = 0$ coming from (1.8) immediately gives the third boundary condition $\frac{\partial \hat{w}_k}{\partial z} = 0$. Finally, taking $\partial/\partial z$ of the equation above and applying the result to (1.12) we get the fourth boundary condition

$$\left.\frac{\partial^2 \hat{w}_k}{\partial z^2}\right|_{z=1} = -k^2 \mathrm{Ma} \hat{T}_k(1,t). \tag{1.22}$$

As stated in [9], the solution for this boundary value problem is

$$\hat{w}_k(z,t) = -\mathrm{Ma}\hat{T}_k(1,t) f_k(z) \tag{1.23}$$

where a function $f_k(z)$ is defined as follows

$$f_k(z) = \frac{k \sinh k}{2(\sinh k \cosh k - k)} \left[kz \cosh(kz) - \sinh(kz) + (1 - k\cosh k) z \sinh(kz)\right]. \tag{1.24}$$

This function plays an essential role in our investigation, so its structure and behaviour will be considered in much more detail in the following chapters. However, it should noted now that the graph and description of $f_k(z)$ presented in [9] is made with an incorrect sign: $f_k(z)$ is in fact a non-positive function of $z \in [0,1]$ and $k \geq 0$.

1.2 Background profile method

Hagstrom and Doering in [9] adapted the background flow method for the case of Pearson's model to formulate a variational upper bound for Nusselt number. Namely, the temperature field is decomposed as follows

$$T = \tau(z) + \theta(\boldsymbol{x}, t) \tag{1.25}$$

where $\tau(z)$ is a background profile and $\theta(\boldsymbol{x}, t)$ is a fluctuation. According to (1.9) and (1.11) the following boundary conditions are imposed on $\tau(z)$

$$\tau(0) = 0, \tag{1.26}$$

$$\tau'(1) = -1 \tag{1.27}$$

whereas $\theta(\boldsymbol{x}, t)$ is equipped with the corresponding homogeneous boundary conditions

$$\theta|_{z=0} = 0, \tag{1.28}$$

$$\left.\frac{\partial \theta}{\partial z}\right|_{z=1} = 0. \tag{1.29}$$

Substituting (1.25) into the equation of heat convection (1.7) gives

$$\frac{\partial\theta}{\partial t} + w\frac{d\tau}{dz} + \boldsymbol{u}\cdot\nabla\theta = \frac{d^2\tau}{dz^2} + \nabla^2\theta. \tag{1.30}$$

It was shown by Hagstrom and Doering in [9] that for a Nusselt number expressed as

$$\frac{1}{\mathrm{Nu}} = \langle|\nabla T|^2\rangle \tag{1.31}$$

one can derive from (1.30) the expression

$$\frac{1}{\mathrm{Nu}} = \int_0^{2\pi}\int_0^1 \left[\left(\frac{\partial\theta}{\partial x}\right)^2 + \left(\frac{\partial\theta}{\partial z}\right)^2 + 2\tau' w\theta\right] dxdz - 2\tau(1) - \int_0^1 \tau'^2 dz \tag{1.32}$$

where the prime denotes a derivative with respect to z. Therefore, we can argue that, given appropriate $\tau(z)$, if the term

$$Q_\tau[\theta] := \int_0^{2\pi}\int_0^1 \left[\left(\frac{\partial\theta}{\partial x}\right)^2 + \left(\frac{\partial\theta}{\partial z}\right)^2 + 2\tau' w\theta\right] dxdz \tag{1.33}$$

is non-negative for all $\theta(\boldsymbol{x}, t)$ satisfying the boundary conditions (1.28), (1.29), then there exists an upper bound for Nusselt number defined as

$$\frac{1}{\mathrm{Nu}} \geq -2\tau(1) - \int_0^1 \tau'^2 dz =: -\mathcal{B}[\tau]. \tag{1.34}$$

As θ also satisfies the periodic boundary condition in the x-coordinate, it can be expanded into Fourier series

$$\theta(\boldsymbol{x}, t) = \sum_{k=-\infty}^{+\infty} \hat{\theta}_k(z, t)e^{ikx}. \tag{1.35}$$

Therefore, employing the property of orthogonality of Fourier series and the fact that $\hat{w}_k^* = \hat{w}_{-k}$ and $\hat{\theta}_k^* = \hat{\theta}_{-k}$ for real-valued functions w and θ, non-negativity of quadratic form $Q_\tau[\theta]$ transforms to condition

$$\frac{1}{2}\int_0^1 \left[\left|\frac{d\hat{\theta}_0}{dz}\right|^2 + 2\tau' Re(\hat{w}_0^*\hat{\theta}_0)\right] dz + \sum_{k=1}^{\infty}\int_0^1 \left[\left|\frac{d\hat{\theta}_k}{dz}\right|^2 + k^2\left|\hat{\theta}_k\right|^2 + 2\tau' Re(\hat{w}_k^*\hat{\theta}_k)\right] dz \geq 0. \tag{1.36}$$

The first term corresponding to $k = 0$ is trivially positive because $\hat{w}_0 = 0$. We thus require that for every $k \geq 1$ the following quantity must be non-negative in order to guarantee that $Q_\tau[\theta] \geq 0$ is satisfied

$$Q_{\tau,k}[\hat{\theta}_k] := \int_0^1 \left[\left|\hat{\theta}_k'\right|^2 + k^2\left|\hat{\theta}_k\right|^2 + 2\tau' Re(\hat{w}_k^*\hat{\theta}_k)\right] dz \geq 0. \tag{1.37}$$

It is referred to as a spectral constraint and essentially provides a stability condition for a chosen background profile $\tau(z)$ in terms of Fourier modes.

Since the only requirement on $\tau(z)$ is that it has to satisfy the boundary conditions (1.26) and (1.27), we want to find such a background profile $\tau(z)$ that an upper bound on Nusselt number defined by (1.34) is minimized. This finally leads to an infinite-dimensional optimization problem

$$\begin{aligned} \min_{\tau} \ \mathcal{B}[\tau] &= 2\tau(1) + \int_0^1 \tau'^2 dz \qquad (1.38)\\ \text{subject to } Q_{\tau,k}[\hat{\theta}_k] &= \int_0^1 \left[\left|\hat{\theta}_k'\right|^2 + k^2 \left|\hat{\theta}_k\right|^2 - 2\mathrm{Ma}\tau' f_k(z) Re(\hat{\theta}_k^*(1)\hat{\theta}_k) \right] dz \geq 0 \text{ for all } k \geq 1 \\ \text{for all } \hat{\theta}_k &\in \mathcal{C}^1(0,1), \hat{\theta}_k(0) = 0, \hat{\theta}_k'(1) = 0, \\ \tau &\in \mathcal{C}^1(0,1), \tau(0) = 0, \tau'(1) = -1. \end{aligned}$$

Using a simple piecewise linear background profile

$$\tau(z) = \begin{cases} -z, \text{ if } 0 \leq z < \delta_1, \\ -\delta_1, \text{ if } \delta_1 \leq z < 1 - \delta_2, \\ -\delta_1 - z + 1 - \delta_2, \text{ if } 1 - \delta_2 \leq z \leq 1. \end{cases} \qquad (1.39)$$

and assuming that the boundary layer $1-\delta_2 \leq z \leq 1$ is infinitesimally small, Hagstrom and Doering in [9] solved the optimization problem (1.38) and obtained a rigorous upper bound on Nusselt number stated in (1.4). Our purpose is to improve their result by means of finding numerically an optimal background profile resulting from the infinite-dimensional optimization problem and then by mathematical analysis of the results of numerical investigation.

1.3 Semidefinite programming

As it will be shown in the next chapter, the optimization problem (1.38) can be expressed as a finite-dimensional semidefinite program. According to [17] a problem is called a semidefinite program in an inequality form if it can be represented as

$$\min_{\boldsymbol{x}} \ \boldsymbol{c}^T \boldsymbol{x} \qquad (1.40)$$

$$\text{subject to } F_0 + \sum_{i=1}^{n} x_i F_i \preccurlyeq 0 \qquad (1.41)$$

where $\boldsymbol{x} \in \mathbb{R}^n$ is a variable, $F_0, F_1, ..., F_N \in \mathbb{R}^{k\times k}$ are constant symmetric matrices, $\boldsymbol{c} \in \mathbb{R}^n$ is a constant vector.

Denotion "$\preccurlyeq 0$" means that the matrix in the left-hand side of (1.41) has to be negative semidefinite. A matrix M is called positive or negative semidefinite if $\boldsymbol{x}M\boldsymbol{x}^T \geq 0$ or $\boldsymbol{x}M\boldsymbol{x}^T \leq 0$ respectively for any vector $\boldsymbol{x} \neq \boldsymbol{0}$. Then, a semidefinite program implies a linear objective function subjected to a set of affine matrices required to be positive/negative semidefinite.

The full form of a semidefinite program also includes an equality constraint $A\boldsymbol{x} = \boldsymbol{b}$. However, as it will not appear in our considerations, it is sufficient to focus on an inequality form of a SDP. The constraint (1.41) is referred to as a linear matrix inequality (LMI). It is also known from [17] that the

same optimization problem subjected to multiple linear matrix inequalities can be expressed as a SDP as well by constructing a block diagonal matrix made of these LMIs.

One should note that the following matrix semidefinite constraint

$$F(\boldsymbol{x}) \succcurlyeq 0 \tag{1.42}$$

can be expressed as a LMI if $F(\boldsymbol{x})$ is a symmetric matrix and every entry of $F(\boldsymbol{x})$ depends linearly on $\boldsymbol{x}$, that is

$$F(\boldsymbol{x}) = \begin{bmatrix} \boldsymbol{c_{11}^T x} & \dots & \boldsymbol{c_{1n}^T x} \\ \vdots & \vdots & \vdots \\ \boldsymbol{c_{n1}^T x} & \dots & \boldsymbol{c_{nn}^T x} \end{bmatrix} \tag{1.43}$$

where $\boldsymbol{c_{ij}}, \boldsymbol{x} \in \mathbb{R}^n$. This fact will be of use in the next chapter.

Due to the development of interior point methods [19], optimization problems expressed in the form of SDP can be solved very efficiently even when a problem's size is large. There are many codes devoted to numerical solving of SDPs. One of the most convenient options is YALMIP, a high-level framework for modelling and solving various optimization problems including semidefinite programs [18]. It allows to express an optimization problem in a simple, user-friendly form and, being equipped by a solver implementing a particular numerical algorithm, solve it. In this work we use a solver SeDuMi recommended by YALMIP documentation for semidefinite programs of medium size. This solver uses an interior point method [19] for numerical solving of SDPs.

Numerical investigation

2.1 Piecewise semidefinite optimization

Before describing an implementation of numerical approach we shall reformulate the problem to make it suitable for recast in the form (1.40), (1.41). The integral inequality (1.37) can be written as

$$Q_{\tau,k}[\hat{\theta}_k] = \int_0^1 \left[Re(\hat{\theta}_k')^2 + k^2 Re(\hat{\theta}_k)^2 - 2\mathrm{Ma}\tau' f_k(z) Re(\theta_k(1)) Re(\hat{\theta}_k) \right] dz \tag{2.1}$$

$$+ \int_0^1 \left[Im(\hat{\theta}_k')^2 + k^2 Im(\hat{\theta}_k)^2 - 2\mathrm{Ma}\tau' f_k(z) Im(\theta_k(1)) Im(\hat{\theta}_k) \right] dz \geq 0. \tag{2.2}$$

If we are required to make these integrals non-negative separately, the whole inequality would be also non-negative. It is therefore sufficient to require that the following functional is non-negative

$$Q_{\tau,k}[u] = \int_0^1 \left[u'^2 + k^2 u^2 - 2\mathrm{Ma}\tau' f_k(z) u u(1) \right] dz \geq 0 \tag{2.3}$$

for any $u(z) \in \mathcal{C}^1(0,1)$ satisfying $u(0) = 0$ and $u'(1) = 0$. Then, the functional $\mathcal{B}[\tau]$ can be expressed only in terms of τ' if we make use of boundary condition $\tau(0) = 0$

$$\mathcal{B}[\tau] = \int_0^1 \left[2\tau' + \tau'^2 \right] dz. \tag{2.4}$$

Out of convenience related to the further use of Legendre series in the current section, we shift the domain in the z-coordinate to $[-1, 1]$ by changing a variable: $\zeta = 2z - 1$. Therefore, the following transformations must be performed:

$$\begin{aligned} dz &= \frac{1}{2} d\zeta, \\ \frac{d\tau}{dz} &= \frac{d\tau}{d\zeta}\frac{d\zeta}{dz} = 2\frac{d\tau}{d\zeta}, \\ \frac{du}{dz} &= 2\frac{du}{d\zeta}. \end{aligned} \tag{2.5}$$

Substituting them into (2.3) and (2.4) gives the final form of infinite-dimensional optimization problem

$$\min_{\tau} \mathcal{B}[\tau] = 2\int_{-1}^{1} \left[\tau' + \tau'^2\right] d\zeta, \tag{2.6}$$

$$\text{subject to } Q_{\tau,k}[u] = \int_{-1}^{1} \left[2u'^2 + \frac{k^2}{2}u^2 - 2\mathrm{Ma}\tau' f_k u u(1)\right] d\zeta \geq 0 \text{ for all } k \geq 1,$$

$$\text{for all } u \in \mathcal{C}^1(-1,1), u(-1) = 0, u'(1) = 0,$$

$$\tau \in \mathcal{C}^1(-1,1), \tau(-1) = 0, \tau'(1) = -\frac{1}{2}.$$

To avoid any confusion, in the remaining part of the section we will use all functions as functions of ζ-coordinate. Derivatives in a short form, i.e. u', are implied to be with respect to ζ. If we need to use a function in the z-coordinate, it will be explicitly stated: for example, $u(z)$ means $u : [0,1] \to \mathbb{R}$, contrary to u or $u(\zeta)$ meaning $u : [-1,1] \to \mathbb{R}$. Denotion f_k implies $f_k(1/2(1+z))$. In other sections we implicitly assume that all functions are defined in the z-coordinate.

In order to transform the problem (2.6) into finite-dimensional form, a relaxation of u, u' by means of Legendre series inspired by Fantuzzi and Wynn approach in [20] is used. This choice is motivated by the fact that Legendre polynomials constitute an orthogonal set of functions allowing to represent the integrals of the first two terms in $Q_{\tau,k}[u]$ as merely algebraic sums which will be shown further. It can be noted that the variational problem (2.6) is formulated with respect to τ' only which means that a finite-dimensional approximation is necessary for τ'. Moreover, for the same reason the boundary condition $\tau(-1) = 0$ does not affect the optimization problem and is used only for calculating τ from τ' by integration. We could also use the Legendre series expansion for τ' and then, assuming that f_k is also expanded into Legendre series, remove the third integral term in $Q_{\tau,k}[u]$ by using a formula for an integral of a product of three Legendre polynomials. However, unlike this approach used in [20], a function τ' is represented as a piecewise constant function defined at equally-spaced mesh because it allows to provide more control on τ'. It will be appreciated later when we discuss the results in the section 2.4.

Hence, we introduce the following series expansions for u, u'

$$u = \sum_{n=0}^{\infty} \hat{u}_n L_n(\zeta), \tag{2.7}$$

$$u' = \sum_{n=0}^{\infty} \hat{u}'_n L_n(\zeta), \tag{2.8}$$

where L_n denotes Legendre polynomial of n-order, $\hat{u}_n, \hat{u}'_n \in \mathbb{R}$ and a prime in Legendre coefficients $\hat{u}'_n$ is used to emphasize that they belong to expansions of u' and does not denote an actual derivative with respect to ζ. It is known from [20] that the Legendre coefficients of expansions of a function and its derivative are related to each other as

$$\hat{u}_0 = u(-1) + \hat{u}'_0 - \frac{\hat{u}'_1}{3} = \hat{u}'_0 - \frac{\hat{u}'_1}{3}, \tag{2.9}$$

$$\hat{u}_n = \frac{\hat{u}'_{n-1}}{2n-1} - \frac{\hat{u}'_{n+1}}{2n+3},$$

where the boundary condition $u(-1) = 0$ has been employed.

As we will see from the numerical results in the section 2.4, a background profile τ' has three distinctive parts: left, middle and right parts. It turned out that its middle part is nearly zero for all Marangoni numbers larger than 10^4. Thus, it is reasonable to set an intermediate region of τ' to zero beforehand separating left and right parts which can be set as piecewise constant functions as sketched in the figure 2.1.

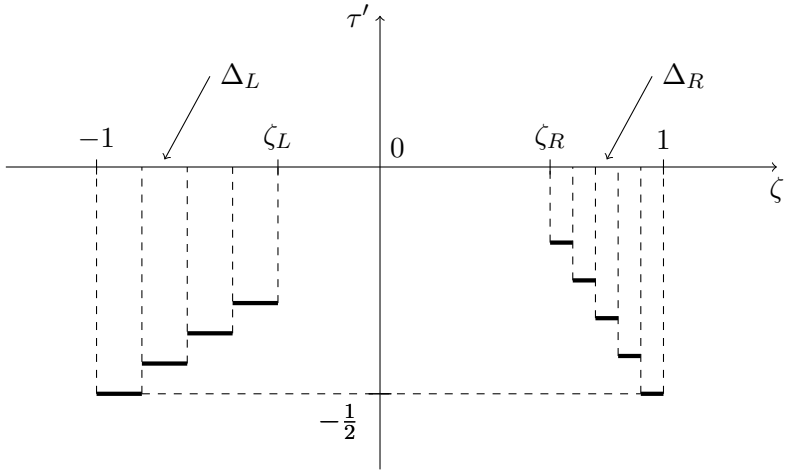

Figure 2.1: Piecewise constant approximation for τ'

As a result, we come to the following form of τ'

$$\tau'(\zeta) = \begin{cases} k_{L,1}, & -1 \le \zeta \le -1 + \Delta_L, \\ \dots & \\ k_{L,N_L}, & -1 + (N_L - 1)\Delta_L < \zeta \le \zeta_L, \\ 0, & \zeta_L < \zeta \le \zeta_R, \\ k_{R,1}, & \zeta_R < \zeta \le \zeta_R + \Delta_R, \\ \dots & \\ k_{R,N_R}, & \zeta_R + (N_R - 1)\Delta_R < \zeta \le 1. \end{cases} \tag{2.10}$$

where ζ_L and ζ_R are bounds of the left and right parts of τ'. Parameters N_L and N_R define the number of finite intervals for the left and right sides. Mesh sizes are calculated from the given parameters: $\Delta_L := (\zeta_L + 1)/N_L$, $\Delta_R := (1 - \zeta_R)/N_R$. Such a definition of τ' allows to refine the mesh size for the left and right parts independently. The boundary condition $\tau'(1) = -1/2$ is imposed by simply setting $k_{R,N_R} = -1/2$.

Substituting the piecewise approximation for τ' into $\mathcal{B}[\tau(\zeta)]$ gives its finite-dimensional form

$$\mathcal{B}(\boldsymbol{k_L}, \boldsymbol{k_R}) = 2\Delta_L \boldsymbol{k_L}^T \boldsymbol{k_L} + 2\Delta_R \boldsymbol{k_R}^T \boldsymbol{k_R} + 2\Delta_L \mathbf{1}^T \boldsymbol{k_L} + 2\Delta_R \mathbf{1}^T \boldsymbol{k_R} \tag{2.11}$$

where $\mathbf{1}$ is a vector of all ones with a corresponding for multiplication dimension. Since semidefinite programming requires to use a linear objective function, we remove the quadratic terms by introducing

two slack variables together with Schur complements. It is known [17] that a minimization of (2.11) is equivalent to a minimization of

$$\mathcal{B}(\boldsymbol{k_L}, \boldsymbol{k_R}, \eta_L, \eta_R) = \eta_L + \eta_R + 2\Delta_L \mathbf{1}^T \boldsymbol{k_L} + 2\Delta_R \mathbf{1}^T \boldsymbol{k_R} \tag{2.12}$$

subjected to a positive semidefiniteness of the following matrices

$$S_L := \begin{bmatrix} \operatorname{diag}(2/\Delta_L) & \boldsymbol{k_L} \\ \boldsymbol{k_L}^T & \eta_L \end{bmatrix} \succcurlyeq 0, \tag{2.13}$$

$$S_R := \begin{bmatrix} \operatorname{diag}(2/\Delta_R) & \boldsymbol{k_R} \\ \boldsymbol{k_R}^T & \eta_R \end{bmatrix} \succcurlyeq 0, \tag{2.14}$$

where η_L and η_R are slack variables, S_L and S_R are so called Schur complements.

After substitution of Legendre series and τ' the quadratic form becomes

$$\begin{aligned} Q(\hat{\boldsymbol{u}}', \hat{\boldsymbol{u}}, \boldsymbol{k_L}, \boldsymbol{k_R}) = 2\sum_{n=0}^{\infty}\sum_{m=0}^{\infty} \hat{u}'_n \hat{u}'_m \int_{-1}^{1} L_n(\zeta) L_m(\zeta) d\zeta \\ + \frac{k^2}{2}\sum_{n=0}^{\infty}\sum_{m=0}^{\infty} \hat{u}_n \hat{u}_m \int_{-1}^{1} L_n(\zeta) L_m(\zeta) d\zeta \\ - 2\mathrm{Ma}\sum_{n=0}^{\infty}\sum_{m=0}^{\infty} \hat{u}_n \hat{u}_m \left(\sum_{p=1}^{N_L} k_{L,p} I^L_{n,p} + \sum_{p=1}^{N_R} k_{R,p} I^R_{n,p} \right) \end{aligned} \tag{2.15}$$

where $I^L_{n,p}$, $I^R_{n,p}$ are defined as follows

$$I^L_{n,p} := \int_{-1+(p-1)\Delta_L}^{-1+p\Delta_L} L_n(\zeta) f_k(\zeta) d\zeta, \tag{2.16}$$

$$I^R_{n,p} := \int_{\zeta_R+(p-1)\Delta_R}^{\zeta_R+p\Delta_R} L_n(\zeta) f_k(\zeta) d\zeta. \tag{2.17}$$

Orthogonality of Legendre polynomials implies that

$$\int_{-1}^{1} L_n(\zeta) L_m(\zeta) d\zeta = \frac{2}{2n+1}\delta_{nm} \tag{2.18}$$

for all $n, m \geq 0$. Therefore, the first two terms in the quadratic form become infinite algebraic sums. Unlike an approach presented in [20] we truncate infinite sums without any additional analysis of the remaining parts. It will not cause any significant issues and only force us to consider more Legendre coefficients to get more smooth profiles than if we employed the technique suggested by Fantuzzi and Wynn. Hence, assuming that we consider Legendre polynomials only up to $N_{u'}$ and N_u orders for u and u' expansions respectively, the quadratic form transforms to

$$Q(\hat{\boldsymbol{u}}', \hat{\boldsymbol{u}}, \boldsymbol{k_L}, \boldsymbol{k_R}) = 2\sum_{n=0}^{N_{u'}} \frac{(\hat{u}'_n)^2}{2n+1} + \frac{k^2}{2}\sum_{n=0}^{N_u} \frac{\hat{u}_n^2}{2n+1} - 2\mathrm{Ma}\sum_{n=0}^{N_u}\sum_{m=0}^{N_u} \hat{u}_n \hat{u}_m \left(\sum_{p=1}^{N_L} k_{L,p} I^L_{n,p} + \sum_{p=1}^{N_R} k_{R,p} I^R_{n,p} \right). \tag{2.19}$$

It can be rewritten in a matrix form

$$Q(\hat{\boldsymbol{u}}', \hat{\boldsymbol{u}}, \boldsymbol{k_L}, \boldsymbol{k_R}) = 2\hat{\boldsymbol{u}}'^T L_{u'} \hat{\boldsymbol{u}}' + \frac{k^2}{2} \hat{\boldsymbol{u}}^T L_u \hat{\boldsymbol{u}} - 2\mathrm{Ma} \hat{\boldsymbol{u}}^T \left(I_L \boldsymbol{k_L} \mathbf{1}^T + I_R \boldsymbol{k_R} \mathbf{1}^T \right) \hat{\boldsymbol{u}} \tag{2.20}$$

where $L_{u'}, L_u := \mathrm{diag}(\frac{2}{2n+1})$ are diagonal matrices and $I_L := (I^L_{n,p}), I_R := (I^R_{n,p})$ are matrices of the integrals.

Using the relations (2.9) we can express $\hat{\boldsymbol{u}}$ as $\hat{\boldsymbol{u}} = T_u \hat{\boldsymbol{u}}'$ where T_u is defined as follows

$$T_u := \begin{bmatrix} 1 & -1/3 & 0 & \dots & 0 \\ 1 & 0 & -1/5 & \dots & 0 \\ \vdots & \ddots & \ddots & \ddots & \vdots \\ 0 & \dots & 1/(2N_u - 1) & 0 & -1/(2N_u + 3) \end{bmatrix} \tag{2.21}$$

which implies that $N_u = N_{u'} - 1$. Then, substituting $T_u \hat{\boldsymbol{u}}'$ instead of $\hat{\boldsymbol{u}}$ into (2.20) gives

$$Q_{\boldsymbol{k_L}, \boldsymbol{k_R}, k}(\hat{\boldsymbol{u}}', \hat{\boldsymbol{u}}) = \hat{\boldsymbol{u}}'^T \left[2L_{u'} + \frac{k^2}{2} T_u^T L_u T_u - 2\mathrm{Ma} T_u^T \left(I_L \boldsymbol{k_L} \mathbf{1}^T + I_R \boldsymbol{k_R} \mathbf{1}^T \right) T_u \right] \hat{\boldsymbol{u}}'. \tag{2.22}$$

By the definition of positive semidefinite matrices, a requirement for this expression to be non-negative is equivalent to a requirement for the matrix inside the brackets to be posivite semidefinite.

Introduce the following matrices

$$Q_{1,k} := 2L_{u'} + \frac{k^2}{2} T_u^T L_u T_u, \tag{2.23}$$

$$Q_{2,k}(\boldsymbol{k_L}, \boldsymbol{k_R}) := 2\mathrm{Ma} T_u^T \left(I_L \boldsymbol{k_L} \mathbf{1}^T + I_R \boldsymbol{k_R} \mathbf{1}^T \right) T_u. \tag{2.24}$$

$$\tag{2.25}$$

As it was mentioned in the introduction, a linear matrix inequality must consist of symmetric matrices whereas the matrix $Q_{2,k}(\boldsymbol{k_L}, \boldsymbol{k_R})$ is non-symmetric. However, it is easy to show that $Q_{2,k}(\boldsymbol{k_L}, \boldsymbol{k_R})$ is positive semidefinite if its symmetric part $\mathrm{sym}(Q_{2,k}) = 1/2 \left[Q_{2,k} + Q^T_{2,k} \right]$ is positive semidefinite. Therefore, we can replace $Q_{2,k}(\boldsymbol{k_L}, \boldsymbol{k_R})$ with its symmetric part without any loss of generality. Then, the final form of constraint is

$$Q_k(\boldsymbol{k_L}, \boldsymbol{k_R}) := Q_{1,k} + 1/2 \left[Q_{2,k} + Q^T_{2,k} \right] \succcurlyeq 0 \tag{2.26}$$

which is a LMI by the argument given in the end of the introduction.

This constraint must be satisfied for all $k \geq 0$. However, it can be shown that there exists such k_{max} that for all $k \geq k_{max}$ the original spectral constraint (2.3) is satisfied. Indeed, if we drop the first term in (2.3) which is always positive and use L^2-norms on $u(z)$ and $u(1)$, we can obtain that the spectral constraint is always satisfied if

$$k \geq 2\mathrm{Ma}^{1/2} ||\tau(z)'||_\infty ||f_k(z)||_\infty =: k_{max} \tag{2.27}$$

where $||\tau(z)'||_\infty$ is expected to be bounded and not growing with respect to Marangoni number and $||f_k(z)||_\infty \approx 0.2$ by definition (1.24). For numerical purposes, we can take empirically $||\tau(z)'||_\infty = 1$ and check it after solving the optimization problem to ensure that all necessary spectral constrains were included into it.

In summary, we have formulated the following semidefinite program

$$\begin{aligned} \min_{\boldsymbol{k_L},\boldsymbol{k_R},\eta_L,\eta_R} \quad & \mathcal{B}(\boldsymbol{k_L},\boldsymbol{k_R},\eta_L,\eta_R) \\ \text{subject to } & Q_k(\boldsymbol{k_L},\boldsymbol{k_R}) \succcurlyeq 0 \text{ for all } 1 \le k \le 0.4\mathrm{Ma}^{1/2}, \\ & S_L \succcurlyeq 0, \\ & S_R \succcurlyeq 0, \\ & k_{R,N_R} = -1/2. \end{aligned} \tag{2.28}$$

An upper bound on Nusselt number can be easily calculated given a minimized $\mathcal{B}(\boldsymbol{k_L},\boldsymbol{k_R},\eta_L,\eta_R)$:

$$\mathrm{Nu} \le \frac{-1}{\mathcal{B}_{opt}(\boldsymbol{k_L},\boldsymbol{k_R},\eta_L,\eta_R)}. \tag{2.29}$$

It should be noted that the boundary condition $u'(1) = 0$ is not imposed, because it is still not clear how to do it in terms of finite Legendre series [20]. Thus, we implicitly allow $u'(1)$ to be arbitrary.

2.2 Optimal scaling law for Nusselt number

Following the conclusion of Boeck and Thess in [10] that Nusselt number exhibits a steady scaling with respect to Marangoni number when $\mathrm{Ma} \ge 10^4$, we solve the semidefinite program 2.28 for a sequence of Marangoni numbers from $\mathrm{Ma} = 10^4$ to $\mathrm{Ma} = 10^6$ and get corresponding optimal background profiles τ' from which we can calculate optimal upper bounds on Nusselt number using (2.29). Our choice of the largest Marangoni number $\mathrm{Ma} = 10^6$ is motivated by numerical limitations which will be discussed in the section 2.7. The resulting upper bounds and currently existing scaling laws for Nusselt number are presented in the log-log plot 2.2. The calculated bound clearly obeys the power law which has the following form

$$\mathrm{Nu} \le 0.554\mathrm{Ma}^{0.252}. \tag{2.30}$$

It can be shown that optimal upper bounds on Nusselt number for Marangoni numbers below 10^4 indeed do not obey a power law and, therefore, are out of our interest.

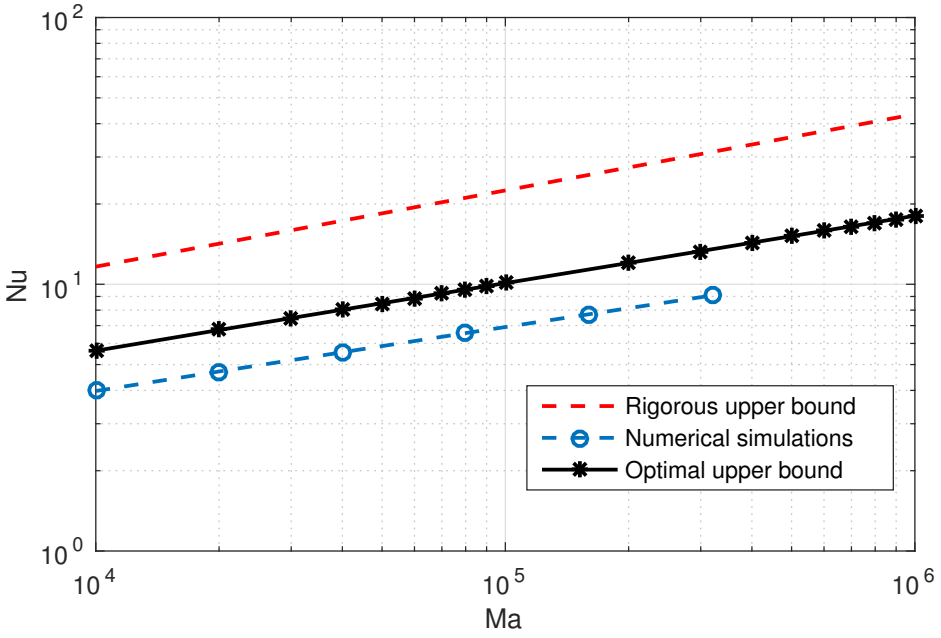

Figure 2.2: Scaling laws for Nusselt number.

We can observe that there are both pre-factor and exponent improvements compared to Hagstrom and Doering rigorous upper bound $\mathrm{Nu} \leq 0.838\mathrm{Ma}^{0.286}$. Moreover, (2.30) is close to the scaling law on Nusselt number obtained from numerical simulations: $\mathrm{Nu} = 0.446\mathrm{Ma}^{0.238}$. The power in (2.30) is slightly higher than 1/4 and gives hope that the true power law's exponent resulting from the infinite-dimensional optimization problem may be 1/4 or even lower taking into account higher Marangoni numbers. This fact will motivate our investigation in the next chapter aimed at analytical improvement of the rigorous upper bound.

2.3 Critical wavenumbers

Before proceeding to an analysis of optimal background profiles, it is important to understand how the constraints in the semidefinite program (2.28) affect the optimization process. Our constraints are in essence the affine matrices required to be positive semidefinite. It is known that a positive semidefinite matrix has non-negative eigenvalues. Therefore, if after finishing optimization of (2.28) some matrices from the constraints have zero eigenvalues, then it is highly likely that the "boundaries" are reached for the corresponding constraints during optimization. Recalling that each constraint and its matrix are related to a particular wavenumber, we can conclude that the corresponding wavenumbers are critical. Hence, it is necessary to look at minimum eigenvalues (also called ground state eigenvalues) of all matrices Q_k with substituted optimal $\boldsymbol{k_L}, \boldsymbol{k_R}$. The resulting plot for different Marangoni numbers and a range of wavenumbers $1 \leq k \lesssim 100$ is presented in the figure 2.3. Ground state eigenvalues continue growing for wavenumbers up to $k = 400$ in a similar manner. Higher wavenumbers were not investigated due to numerical issues which will be discussed in the section 2.7.

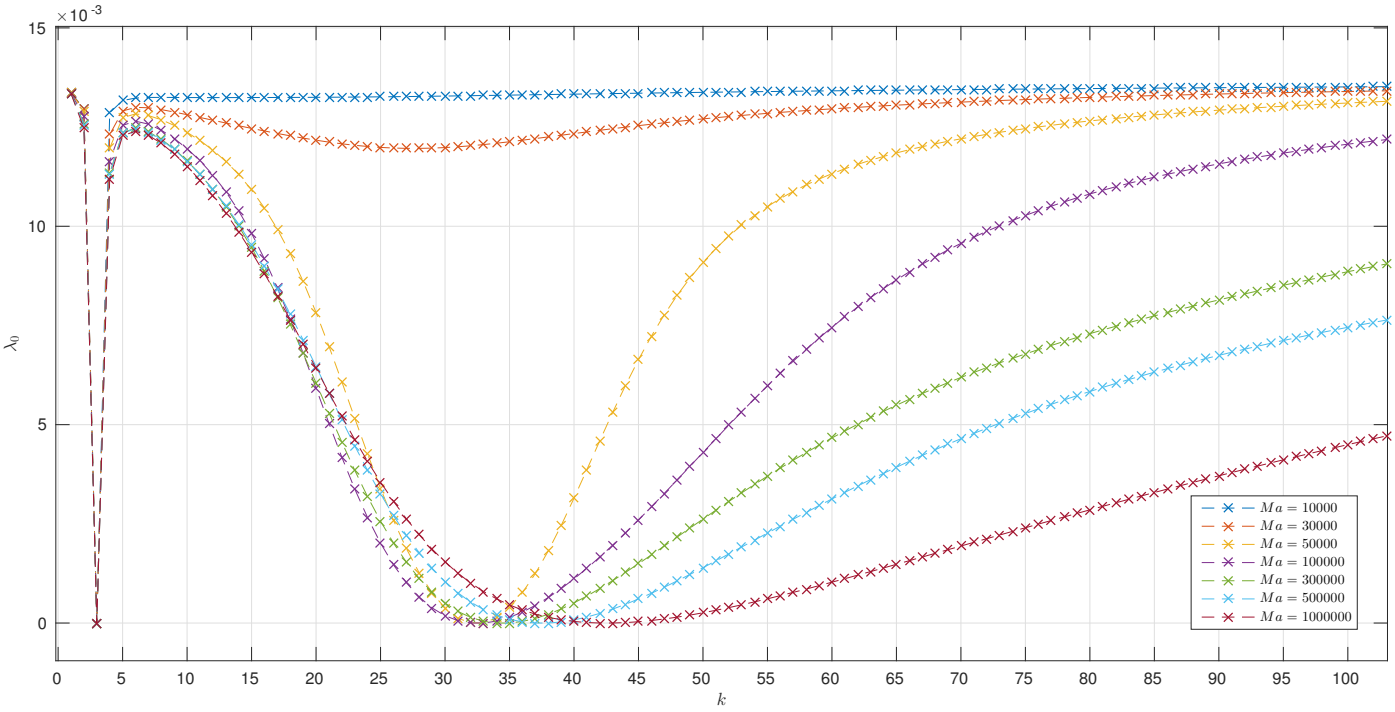

Figure 2.3: Ground state eigenvalues.

It can be observed that for all considered Marangoni numbers there is a critical wavenumber $k = 3$. It is the only zero ground state eigenvalue for relatively low Marangoni numbers, but as Ma increases, a local minima appears on the curve of ground state eigenvalues which tends to zero as Ma grows further until it finally reaches a zero value. It happens at approximately $\text{Ma} = 5 \times 10^4$ where an additional pair of critical wavenumbers appears. If we increase Marangoni number further, these new critical wavenumbers start shifting which is shown in detail in the figure 2.5 and table 2.4.

Marangoni number (Ma)	Critical wavenumbers (k_{cr})	k_{max}
10^4	3	40
5×10^4	$3, 33, 34$	90
10^5	$3, 33, 34$	127
3×10^5	$3, 34, 35$	220
5×10^5	$3, 37, 38$	283
10^6	$3, 42, 43$	400

Figure 2.4: Shift of critical wavenumbers.

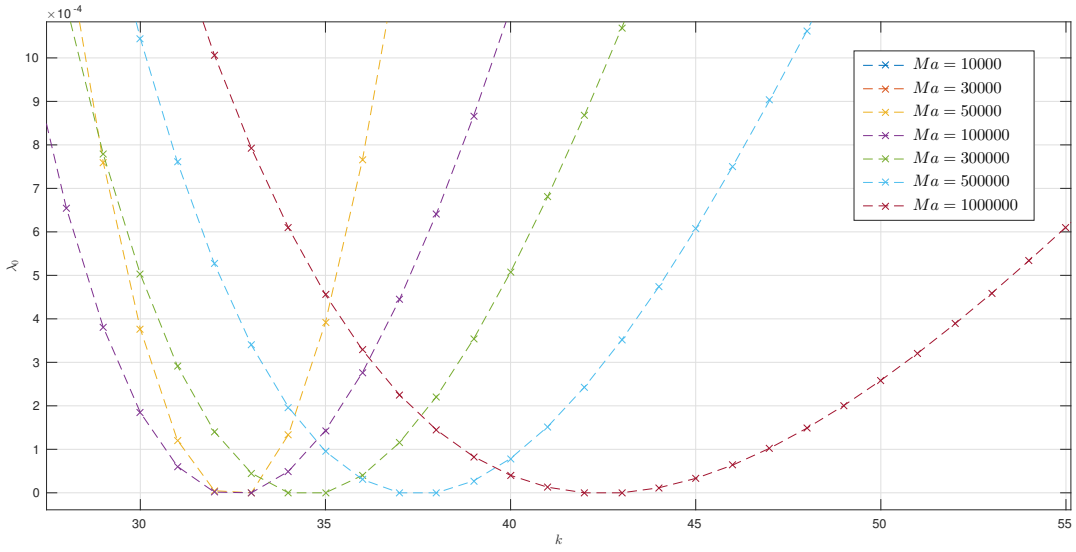

Figure 2.5: A pair of zero ground state eigenvalues.

One can note from the figure 2.3 that for Ma $\geq 5 \times 10^4$ the curve past $k \approx 50$ decreases steadily as Marangoni number grows further which resembles the way the pair of additional critical wavenumbers appears for lower Marangoni numbers. As a result, we can expect that a new pair of critical wavenumbers or a single zero eigenvalue may appear in a similar fashion if we consider Marangoni numbers above 10^6.

It can be also observed from the table 2.4 that the second/third critical wavenumber scale with respect to Marangoni number as approximately $k_{cr} \propto \mathrm{Ma}^{1/10}$ which is significantly lower compared to the analytically calculated maximum wavenumber $k_{max} \propto \mathrm{Ma}^{1/2}$.

We should note one more important point. The second pair of critical wavenumbers can be guessed without considering the whole interval $1 \leq k \leq k_{max}$. In fact, one can carry out calculations for only one wavenumber $k = 3$ (i.e. with only one constraint $Q_3 \succcurlyeq 0$ in (2.28)), see that there is a range of negative ground state eigenvalues, take wavenumbers corresponding to only the two smallest ground state eigenvalues, repeat calculations with constraints corresponding to the selected wavenumbers and $k = 3$ and observe that once these three constraints are satisfied, the whole range of previously negative ground state eigenvalues is now automatically positive. From this behaviour we can conclude the following qualitative algorithm of seeking the optimal solution: the wavenumber $k = 3$ sets the whole profile's structure; after that another critical wavenumber (or a pair of them) is "sought" by the optimization algorithm such that the profile for $k = 3$ is adjusted to become feasible for the whole considered range of wavenumbers.

2.4 Analysis of background profile

Out of convenience we present optimal background profiles τ and τ' in the domain $z \in [0, 1]$. A typical optimal τ together with a simple profile (1.39) used by Hagstrom and Doering in [9] for Ma $= 10^4$ are presented in the figure 2.6. It can be observed that the optimal background profile consist of two distinctive boundary layers with an approximately constant middle part. The resultant left boundary layer is much

larger compared to Hagstrom and Doering profile. The right boundary layer assumed to be negligible in (1.39) is clearly present in optimal τ and has both increasing and decreasing intervals creating thus a double boundary layer at the upper surface.

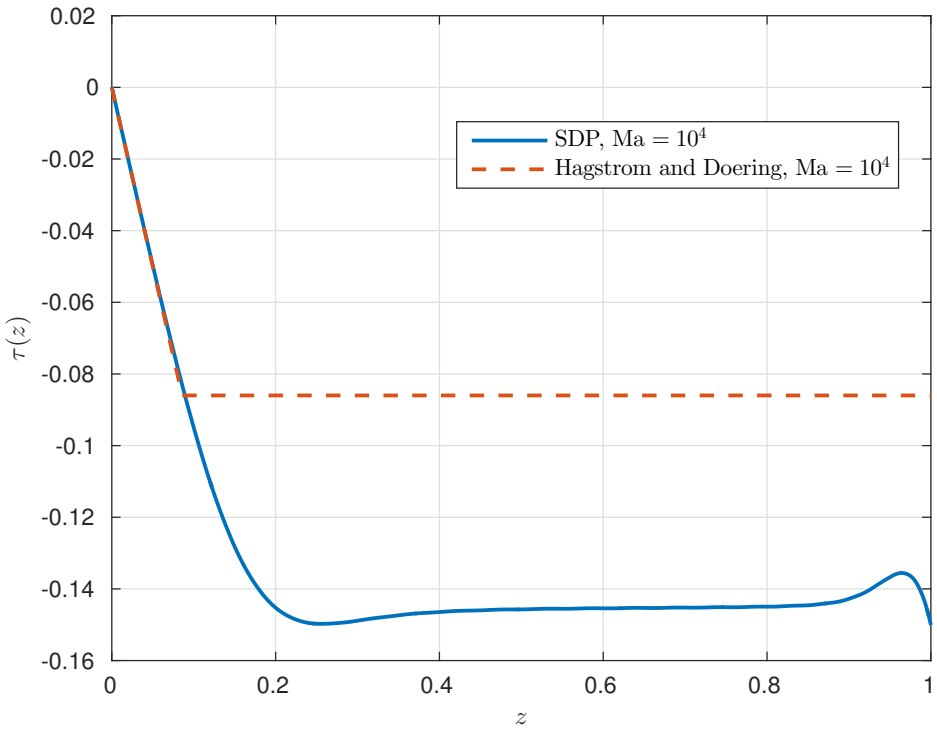

Figure 2.6: Optimal background profile $\tau(z)$ for Ma $= 10^4$ and Hagstrom and Doering profile.

From the mathematical point of view, it is more important to analyse optimal background profiles τ' which are shown in the figure 2.7 for a range of Marangoni numbers from 10^4 up to 2×10^5. It can be clearly observed that the profiles are self-similar and have two distinctive parts: the left part tending to $z = 0$ and the right part tending to $z = 1$ as Ma increases. Furthermore, both parts of τ' seem to collapse as Marangoni number increases. Wavy structure of the right part of τ' profiles is explained by using the finite-dimensional approximation for u and u' and the following truncation of infinite sums compared to [20] where the full form of infinite sums were analysed. However, it does not affect the results significantly and therefore was not employed in this work. For obtaining smooth profiles one could implement the same problem using recently released Matlab code QUINOPT [22].

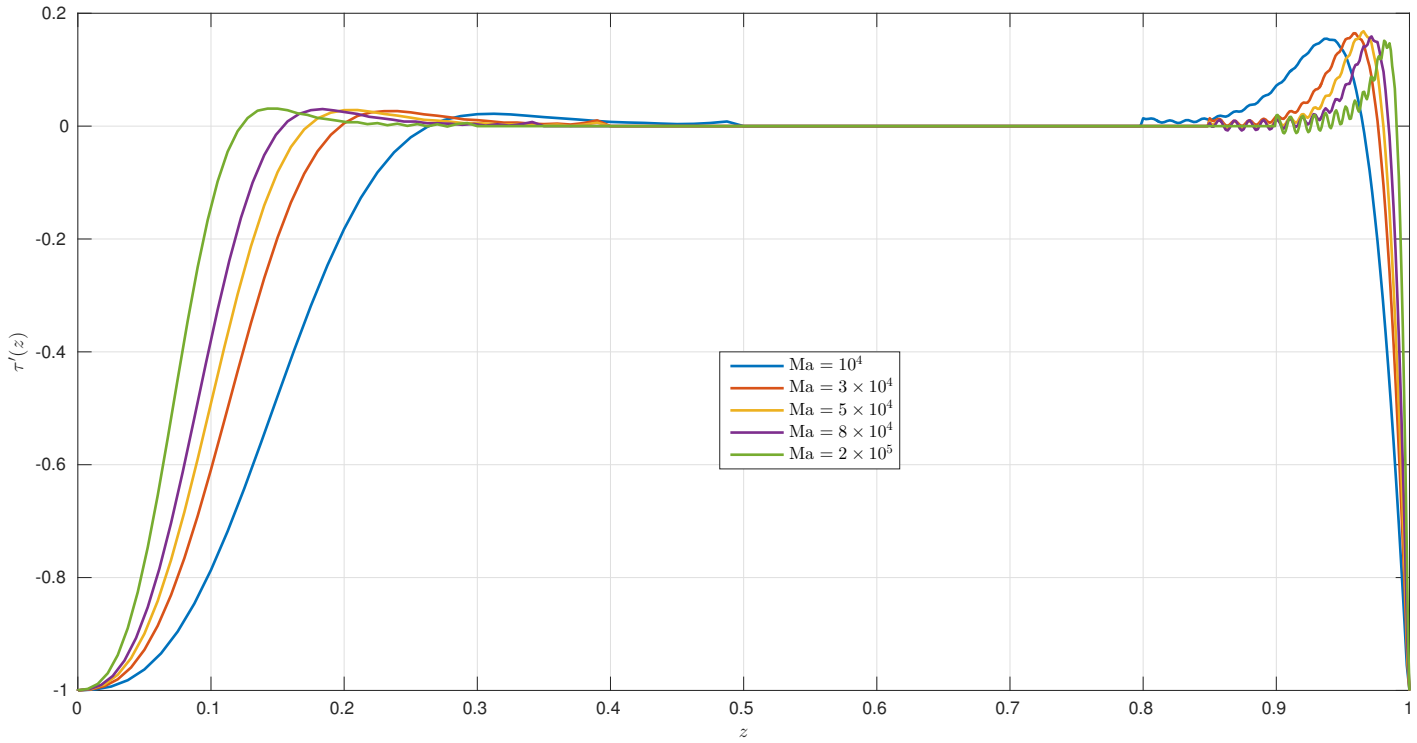

Figure 2.7: Optimal background profiles $\tau'(z)$.

Apart from collapsing, i.e. scaling along the z-coordinate, the left and right parts of τ' profiles also scale vertically with respect to Marangoni number. It can be seen from the figure 2.8 that the pick of the left side exhibits a steady growth as Marangoni number increases. In contrast, the right side's pick rather oscillates around some value than merely grows or decays. It may be possible that these oscillations are linked to the shifting second critical wavenumbers.

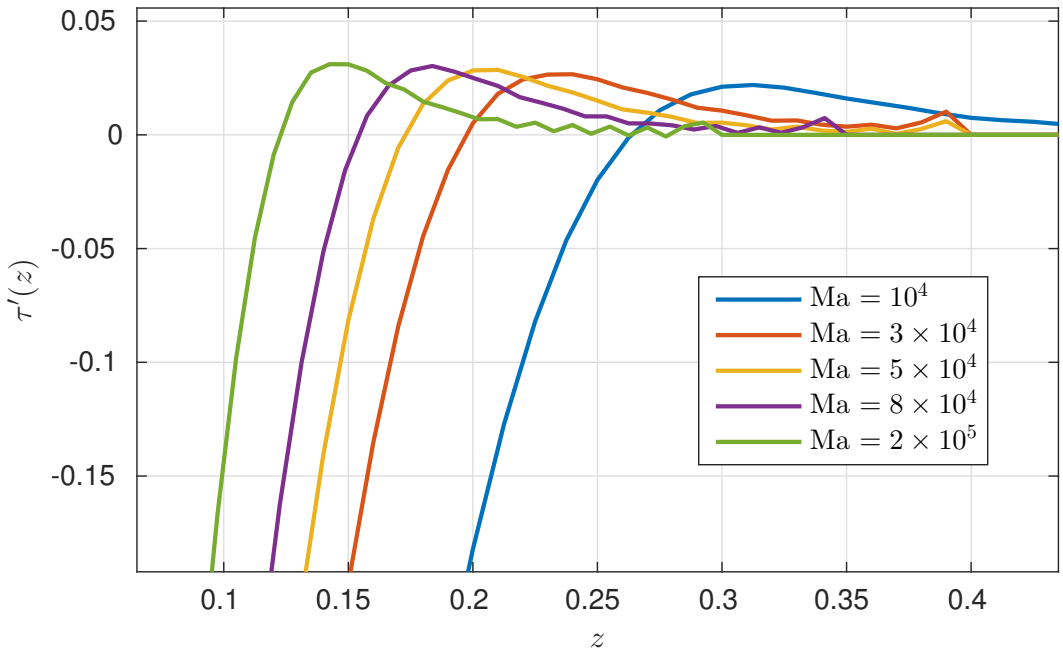

Figure 2.8: Left side of $\tau'(z)$ profiles.

From these results and the investigation of ground state eigenvalues, we can give the following interpretation of the action of critical wavenumbers on a background profile. Firstly, the whole profile's structure is caused by a critical wavenumber $k = 3$. It is not surprising regarding the left part of profiles if we look at $f_k(z)$ for a different range of k carefully. It can be seen from the middle graph in the figure 2.9 that $\max_k f_k(z) = f_3(z)$ for $0 \leq z < 0.5$. Moreover, we can observe from the top plot in the same figure that $f_k(z)$ is nearly zero for $k > 15$ on the same range of z. It means that the third term in the functional $Q_{\tau,k}[u]$ in (2.3) is not affected by $\tau'(z)$ at $0 \leq z < 0.5$ when $k \gtrsim 15$. Therefore, we can argue that the left part of the profile is determined by only $k = 3$ whereas wavenumbers larger than approximately 15 do not affect it whatsoever.

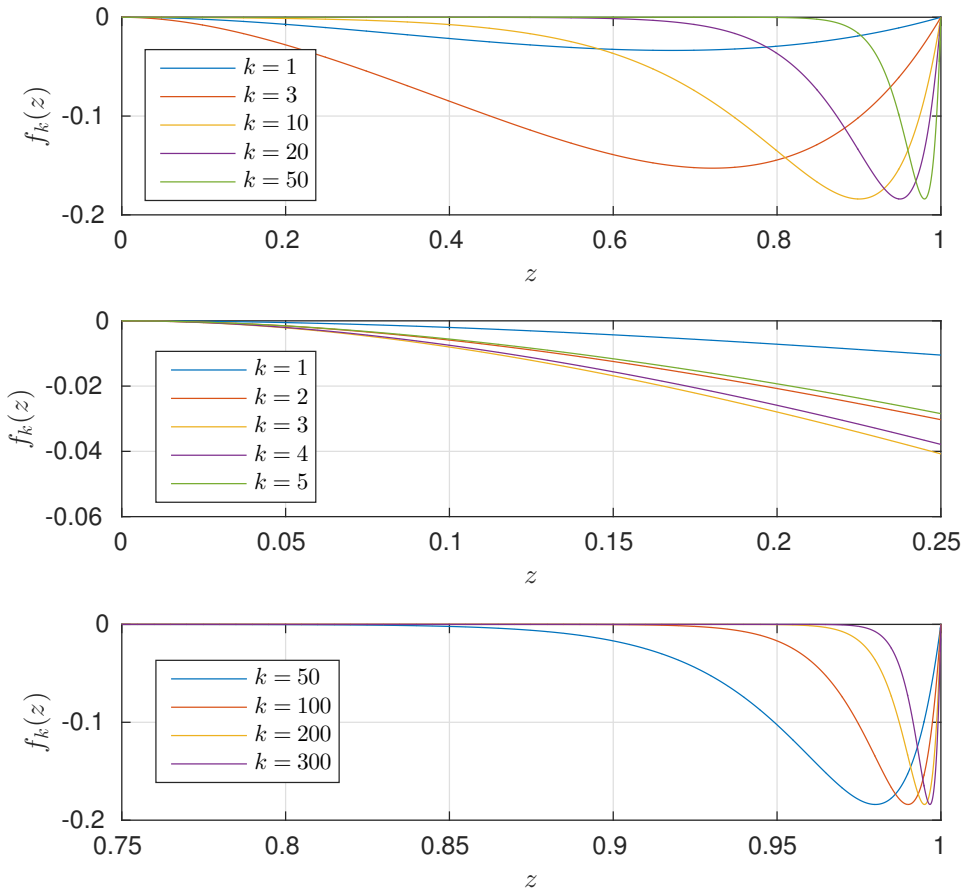

Figure 2.9: Common behaviour of $f_k(z)$ (top), $f_k(z)$ at $0 \leq z \leq 0.25$ (middle) and concentraction of $f_k(z)$ near $z = 1$ (bottom).

What is more interesting, the form of the right part is also determined by the constraint related to the first critical wavenumber $k = 3$. One can observe from the figure 2.10 that the right part similar to what we saw in the figure 2.7 is present when only one constraint corresponding to $k = 3$ is included into the optimization problem (2.28). When we then include two additional constraints corresponding to a pair of higher critical wavenumbers, the right part is slightly adjusted but its structure is not affected qualitatively.

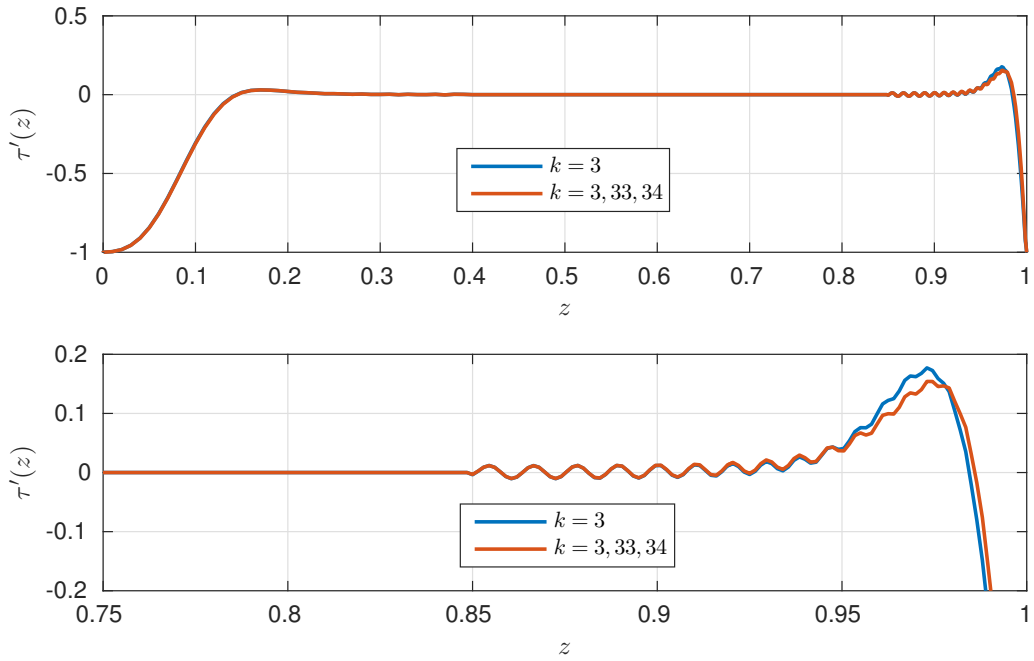

Figure 2.10: Adjustment of $\tau'(z)$ profile for $\mathrm{Ma} = 10^5$ caused by higher critical wavenumbers.

It is important to note that due to a flexibility of the piecewise approximation of τ', we can enforce different conditions on τ' via the coefficients $\boldsymbol{k_L}$, $\boldsymbol{k_R}$ in order to clarify the way the right part of the profile τ' affects the scaling law for an upper bound on Nusselt number. For example, we can imitate the case considered by Hagstrom and Doering in [9] where they assumed that $\tau' \leq 0$ by requiring $k_{L,i} \leq 0$ and $k_{R,i} \leq 0$ which is still a semidefinite program. The resultant optimal background profile τ' for $\mathrm{Ma} = 10^4$ is shown on the third plot in the figure 2.11. It can be observed that the left part is thinner compared to the case of unrestricted $\boldsymbol{k_L}$, $\boldsymbol{k_R}$ located at the top of the same figure. The right boundary layerm in turn becomes extremely tiny.

Furthermore, we can allow the left part set by $\boldsymbol{k_L}$ to be arbitrary, but neglect the right part by enforcing $k_{R,i} = 0$. In this case one can observe from the second graph in the figure 2.11 that the left part is still smaller than in the original case, but bigger than in the case of $\tau' \leq 0$. This result is caused by the positive part of τ' including a sharp positive increase at the boundary of the left part. Moreover, if the boundary is moved by means of changing ζ_L in the SDP, a small positive jump persists.

Hagstrom and Doering profile presented in the bottom of the figure 2.11 exhibits the smallest left part compared to other optimal background profiles.

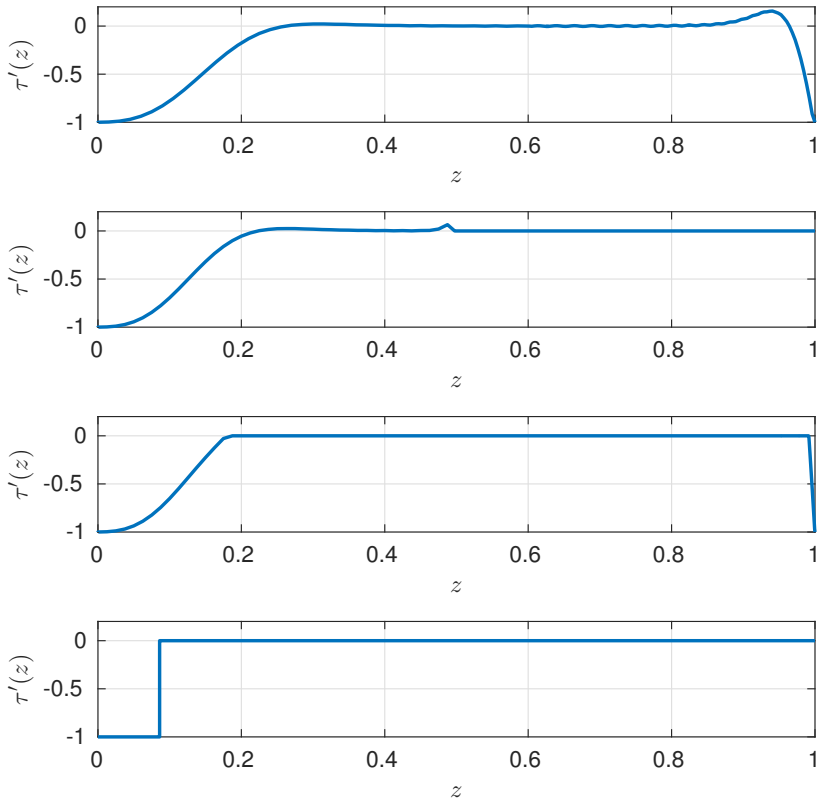

Figure 2.11: $\tau'(z)$ for $\mathrm{Ma} = 10^4$ in the case of general $\boldsymbol{k_L}$, $\boldsymbol{k_R}$ (top), $\boldsymbol{k_R} = \mathbf{0}$ (second from the top), $k_{L,i}, k_{R,i} \leq 0$ (middle), Hagstrom and Doering profile (bottom).

Solving the semidefinite program (2.28) with appropriate constraints for a range of Marangoni numbers, we obtain the following scaling laws

$$\text{Truncated right part: } \mathrm{Nu} \leq 0.441\mathrm{Ma}^{0.295}, \tag{2.31}$$

$$\text{Negative } \tau' \text{: } \mathrm{Nu} \leq 0.420\mathrm{Ma}^{0.305}. \tag{2.32}$$

It is easy to see that these power laws are significantly worse than the fully optimal power law (2.30). Moreover, the exponents (2.31) and (2.32) are even greater than $2/7$ which is the exponent in Hagstrom an Doering power law (1.4). In fact, we suspect that the exponents asymptotically tend to $2/7$. The comparative plot is presented in the figure 2.12. The following conclusions can be deduced from the comparison of optimal background profiles and scaling laws for different cases:

1. the larger left part and a negative segment of the right part of τ' seems to produce the smaller upper bound on Nusselt number;

2. both parts become larger due to a positive part of τ'.

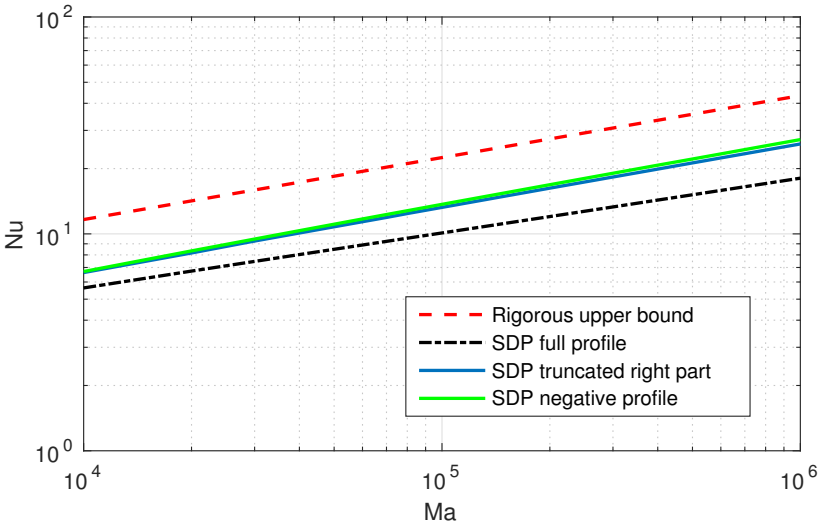

Figure 2.12: Comparison of upper bounds produced by different forms of profiles.

These numerical experiments clearly show an importance of the positivity of the right part. Firstly, it allows the left part which is suggested to be the main contributor in decreasing an upper bound on Nusselt number to be larger. Secondly, it makes the right negative boundary layer wider. As a result, the interplay of the boundary layers produces a significantly lower upper bound on Nusselt number.

2.5 Discontinuous piecewise optimization

From the previous numerical investigation using semidefinite programming we have learnt the importance of the positive right part of τ' profile. It is not meaningless to suggest that we may get a scaling law for Nusselt number similar to the SDP one if we used a simplified piecewise τ' profile similar to the Hagstrom and Doering profile (1.39), but with a fixed positive right part instead of the negative one. Such a simplified profile is shown in the figure 2.13 and has the following expression

$$\tau'(\zeta) = \begin{cases} -1/2, & -1 \le \zeta \le \zeta_L, \\ 0, & \zeta_L \le \zeta \le \zeta_R, \\ \kappa, & \zeta_R \le \zeta \le 1. \end{cases} \tag{2.33}$$

where $\kappa \ge 0$ is some fixed value chosen empirically and ζ_L and ζ_R are to be varied.

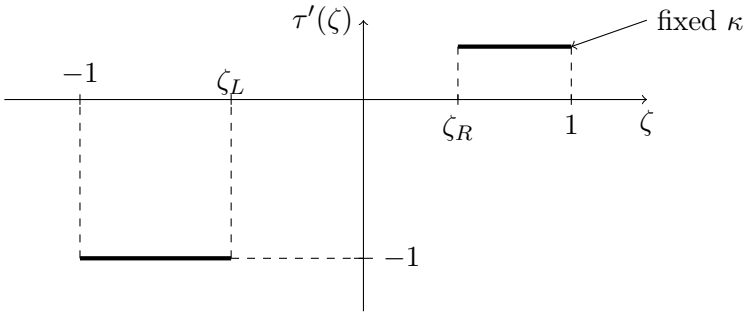

Figure 2.13: The simplified background profile $\tau'(\zeta)$

It leads to a modified optimization problem

$$\min_{\zeta_L,\zeta_R} \frac{1}{2}(\zeta_R-\zeta_L)+2\left(\kappa+\frac{1}{2}\right)^2(1-\zeta_R)-1 \tag{2.34}$$

$$\text{subject to } \int_{-1}^{1}\left[2u'^2+\frac{k^2}{2}u^2\right]d\zeta+\mathrm{Ma}u(1)\int_{-1}^{\zeta_L}uf_k d\zeta-2\kappa\mathrm{Ma}u(1)\int_{\zeta_R}^{1}uf_k d\zeta\geq 0 \text{ for all } 1\leq k\leq 0.4\mathrm{Ma}^{1/2} \tag{2.35}$$

which cannot be solved by means of semidefinite programming. However, optimal solutions are still achievable with a sufficient computational efficiency if we consider a naive algorithm for solving the optimization problem.

In order to transform an integral constraint to a finite-dimensional form, we are going to use the same strategy with Legendre series as in the piecewise SDP, so all repeating details will be skipped. Hence, expanding u and u' in truncated Legendre series gives the following form of the integral constraint

$$2\sum_{n=0}^{N_{u'}}\frac{2(\hat{u}'_n)^2}{2n+1}+\frac{k^2}{2}\sum_{n=0}^{N_u}\frac{2\hat{u}_n^2}{2n+1}-2\mathrm{Ma}\sum_{n=0}^{N_u}\sum_{m=0}^{N_u}\hat{u}_n\hat{u}_m\left[\frac{1}{2}\int_{-1}^{\zeta_L}L_nf_k d\zeta-\kappa\int_{\zeta_R}^{1}L_nf_k d\zeta\right]\geq 0. \tag{2.36}$$

The naive algorithm is based on the idea that we can successively vary ζ_L and ζ_R in a range $-1\leq\zeta_L\leq\zeta_R\leq 1$ such that this inequality is satisfied for all $k\leq k_{max}$ and the objective function (2.34) reaches its minima. It is possible to implement if two remaining integrals are split into finite sums with sufficiently small steps. However, as we can observe from the previous numerical works, the accuracy of the steps must depend on Marangoni number being considered (i.e. steps must decrease as Ma increases) because otherwise we will get too rough solutions and may lose important details of the scaling law. In order to bound the influence of inaccuracy, we will be using guesses for limits of optimal $\zeta_{L,opt}$ and $\zeta_{R,opt}$ for each Marangoni number such that the guesses will depend on Ma. In other words, we say that the following limits can be calculated for every Ma

$$-1\leq\zeta_{L,min}(\mathrm{Ma})<\zeta_{L,opt}(\mathrm{Ma})<\zeta_{L,max}(\mathrm{Ma})\leq 1, \tag{2.37}$$

$$-1\leq\zeta_{R,min}(\mathrm{Ma})<\zeta_{R,opt}(\mathrm{Ma})<\zeta_{R,max}(\mathrm{Ma})\leq 1. \tag{2.38}$$

One could argue that it is hard to construct such limits in general. Even though it is true, we are rather interested in the scaling laws of $\zeta_{L,opt}(\mathrm{Ma})$ and $\zeta_{L,opt}(\mathrm{Ma})$ than their particular values for a given arbitrary

Ma which implies that the optimization problem is solved for a whole array of Marangoni number. Indeed, if we have an equally-spaced sequence of Marangoni numbers $(\mathrm{Ma}_n) = (\mathrm{Ma}_0, \mathrm{Ma}_1, ...)$, then basing on the idea that $\zeta_{L,opt}(\mathrm{Ma}), \zeta_{R,opt}(\mathrm{Ma})$ must collapse as Ma increases, the recursive sequences of limits can be produced

$$\zeta_{L,min}(\mathrm{Ma}_n) = \zeta_{L,opt}(\mathrm{Ma}_{n-1}) - 2[\zeta_{L,max}(\mathrm{Ma}_{n-1}) - \zeta_{L,opt}(\mathrm{Ma}_{n-1})], \tag{2.39}$$

$$\zeta_{L,max}(\mathrm{Ma}_n) = \zeta_{L,opt}(\mathrm{Ma}_{n-1}), \tag{2.40}$$

$$\zeta_{R,min}(\mathrm{Ma}_n) = \zeta_{R,opt}(\mathrm{Ma}_{n-1}), \tag{2.41}$$

$$\zeta_{R,max}(\mathrm{Ma}_n) = \zeta_{R,opt}(\mathrm{Ma}_{n-1}) + 2[\zeta_{L,opt}(\mathrm{Ma}_{n-1}) - \zeta_{R,min}(\mathrm{Ma}_{n-1})]. \tag{2.42}$$

The n-th iteration of this process for the case of ζ_L is demonstrated in the figure 2.14. It is easily seen that if the optimal $\zeta_{L,opt}$ and $\zeta_{R,opt}$ are collapsing with respect to increasing Marangoni number, then the intervals $[\zeta_{L,min}, \zeta_{L,max}]$ and $[\zeta_{R,min}, \zeta_{R,max}]$ are shrinking. Therefore, if we set a constant number of discretization steps , a necessary level of accuracy will be still maintained because smaller and smaller limiting intervals are considered as Ma increases. We only need to set initial guesses for these interval for Ma_0 that can be obtained from the corresponding results in piecewise semidefinite optimization.

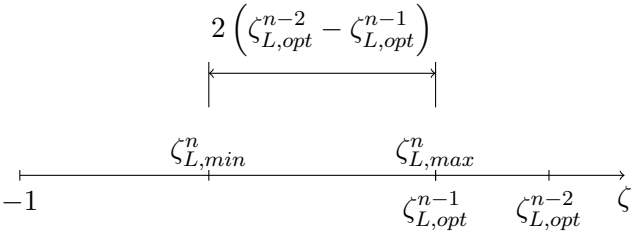

Figure 2.14: Limits of $\zeta_{L,opt}$ for Ma_n

In the light of this discussion, we rewrite the inequality constraint on the quadratic from such that

$$\begin{aligned} &2\sum_{n=0}^{N_{u'}} \frac{2(\hat{u}_n')^2}{2n+1} + \frac{k^2}{2}\sum_{n=0}^{N_u} \frac{2\hat{u}_n^2}{2n+1} \\ &-2\mathrm{Ma}\sum_{n=0}^{N_u}\sum_{m=0}^{N_u} \hat{u}_n\hat{u}_m \left[\frac{1}{2}\left(\int_{-1}^{\zeta_{L,min}} L_n f_k d\zeta + \int_{\zeta_{L,min}}^{\zeta_L} L_n f_k d\zeta\right) - \kappa\left(\int_{\zeta_R}^{\zeta_{R,max}} L_n f_k d\zeta + \int_{\zeta_{R,max}}^{1} L_n f_k d\zeta\right)\right] \geq 0 \end{aligned} \tag{2.43}$$

where $\zeta_{L,min} < \zeta_L \leq \zeta_{L,max}$ and $\zeta_{R,min} \leq \zeta_R < \zeta_{R,max}$.

The integrals not involving ζ_L and ζ_R are not varied in optimization problem, so they can be calculated beforehand. Denote them

$$l_{n,0} := \int_{-1}^{\zeta_{L,min}} L_n f_k d\zeta, \tag{2.44}$$

$$r_{n,0} := \int_{\zeta_{R,max}}^{1} L_n f_k d\zeta, \tag{2.45}$$

and corresponding vectors $\boldsymbol{l_0} := (l_{1,0}, l_{2,0}, ..., l_{N_u,0})^T$, $\boldsymbol{r_0} := (r_{1,0}, r_{2,0}, ..., r_{N_u,0})^T$.

To make the optimization problem finite-dimensional, it is necessary to express integrals involving optimizing variables as finite sums. Suppose that the intervals $[\zeta_{L,min}(\mathrm{Ma}_n), \zeta_{L,max}(\mathrm{Ma}_n)]$ and $[\zeta_{R,min}(\mathrm{Ma}_n), \zeta_{R,max}(\mathrm{Ma}_n)]$ are divided into a constant number of spans: $N_{L,max}$ and $N_{R,max}$ respectively. Then, we have the following mesh sizes for left and right parts

$$\Delta_L := \frac{\zeta_{L,max}(\mathrm{Ma}_n) - \zeta_{L,min}(\mathrm{Ma}_n)}{N_{L,max}}, \tag{2.46}$$
$$\Delta_R := \frac{\zeta_{R,max}(\mathrm{Ma}_n) - \zeta_{R,min}(\mathrm{Ma}_n)}{N_{R,max}},$$

and, therefore, ζ_L and ζ_R can be expressed as $\zeta_L = N_L\Delta_L$ and $\zeta_R = N_R\Delta_R$ which makes $N_L, N_R \in \mathbb{N}$ new optimizing variables. It can be seen from (2.46) that the mesh sizes decrease steadily as the bounding intervals shrink.

Next, we define integrals on each span

$$L_{n,i} := \int_{-1+(i-1)\Delta_L}^{-1+i\Delta_L} L_n f_k d\zeta,\ 1 \le i \le N_L, \tag{2.47}$$
$$R_{n,i} := \int_{\zeta_R+(i-1)\Delta_R}^{\zeta_R+i\Delta_R} L_n f_k d\zeta,\ 1 \le i \le N_R, \tag{2.48}$$

so $L_{n,i}$ and $R_{n,i}$ constitute the corresponding matrices L and R.

Finally, substituting these results into (2.43) gives an inequality

$$2\sum_{n=0}^{N_{u'}} \frac{2\left|u_n'\right|^2}{2n+1} + \frac{k^2}{2}\sum_{n=0}^{N_u} \frac{2\left|u_n\right|^2}{2n+1} - 2\mathrm{Ma}\sum_{n=0}^{N_u}\sum_{m=0}^{N_u} u_n u_m \left[\frac{1}{2}\left(l_{n,0} + \sum_{i=1}^{N_L} L_{n,i}\right) - \kappa\left(r_{n,0} + \sum_{i=1}^{N_R} R_{n,i}\right)\right] \ge 0$$

or, equally, the positive semidefiniteness constraint

$$Q_k(N_L, N_R) := Q_{1,k} + 2MaT_u^T\left[\frac{1}{2}\left(\boldsymbol{l_0} + L\ \boldsymbol{1_L}\right)\boldsymbol{1_u^T} - \kappa\left(\boldsymbol{r_0} + R\ \boldsymbol{1_R}\right)\boldsymbol{1_u^T}\right]T_u \succcurlyeq 0 \tag{2.49}$$

where $\boldsymbol{1_L} \in \mathbb{R}^{N_L}$, $\boldsymbol{1_R} \in \mathbb{R}^{N_R}$, $\boldsymbol{1_u} \in \mathbb{R}^{N_u}$ and $Q_{1,k}$, T_u are defined as in the piecewise SDP.

Integrals $L_{n,i}$ and $R_{n,i}$ can be easily prepared beforehand using Simpson's rule. Even for very small Δ_L and Δ_R it is computationally efficient.

Recalling that our new optimization variables are N_L and N_R, we update the optimization problem:

$$\min_{N_L,N_R}\ \frac{1}{2}(N_R\Delta_R - N_L\Delta_L) + 2\left(\kappa + \frac{1}{2}\right)^2(1 - N_R\Delta_R) - 1 \tag{2.50}$$
$$\text{subject to } Q_k(N_L, N_R) \succcurlyeq 0 \text{ for all } 1 \le k \le 0.4\mathrm{Ma}^{1/2}, \tag{2.51}$$
$$1 \le N_L \le N_{L,max},$$
$$1 \le N_R \le N_{R,max}. \tag{2.52}$$

This is a discontinuous optimization problem. Hence, it is solved by brute force where N_L and N_R are varied successively from 1 to $N_{L,max}$ and $N_{R,max}$ respectively such that (2.51) is satisfied and the objective function (2.50) is minimized. Even though the algorithm is naive and may be significantly improved, its performance has appeared to be sufficient for our purposes.

2.6 Results of discontinuous optimization

The resulting optimal upper bounds on Nusselt number are presented in the figure 2.15 together with available scaling laws for Nusselt number. It can be observed that the upper bounds corresponding to the simplified background profile (2.33) are only slightly above the fully optimal upper bounds coming from the SDP results. It means that our assumption about the significance of the positive right part is correct at least for a range of Marangoni numbers up to 10^6.

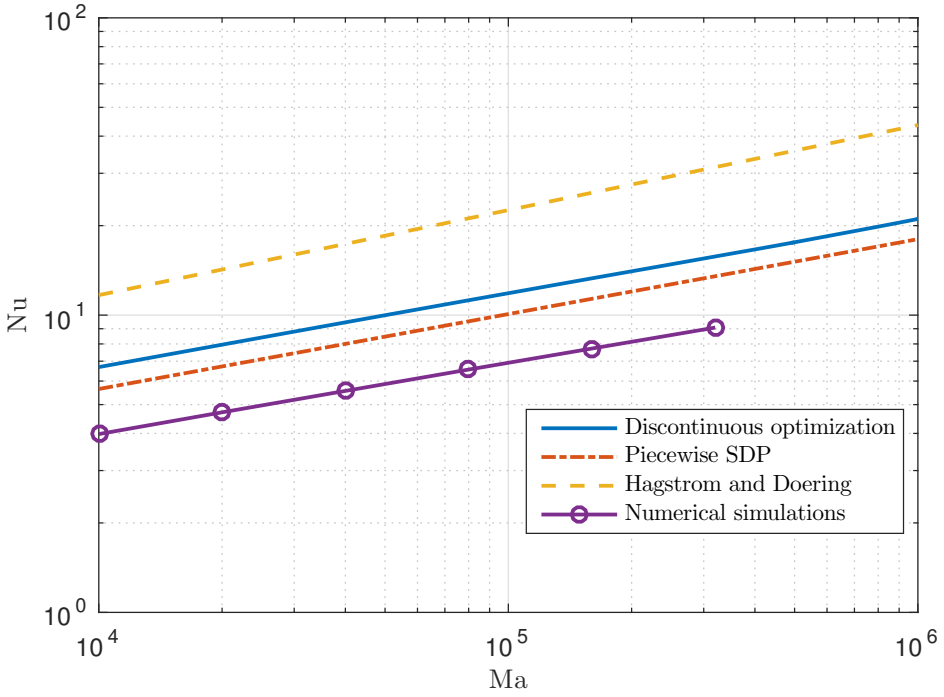

Figure 2.15: Comparison of results of discontinuous optimization to other scaling laws for Nusselt number.

However, the upper bounds resulting from the discontinuous optimization problem do not strictly obey the power law. In fact, it was found that the exponent of the power law becomes dependent on Marangoni number. We investigate it together the scaling laws for boundary layers widths defined by $\delta_L := \zeta_L + 1$ and $\delta_R := 1 - \zeta_R$. We can reasonably assume that $\delta_L(\mathrm{Ma})$ and $\delta_R(\mathrm{Ma})$ as well as an upper bound on Nu obey some power laws at least locally. These local powers can be retrieved if we recall that power laws are merely lines in a log-log scale. Indeed, suppose that we want to calculate a power for a quantity Y obeying locally a power law $Y = cX^\gamma$. Taking the natural logarithm of both sides gives

$$\ln(Y) = \gamma \ln(X) + \ln(c). \tag{2.53}$$

It means that we can calculate γ using linear least-square for a local choice of X and Y in the logarithmic scale. Therefore, given a sequence $(X_n)_{n=1}^N$ and a corresponding sequence $(Y_n)_{n=1}^N$, a local power can be retrieved by solving linear least-square for $[\ln(X_{n-1}), \ln(X_n), \ln(X_{n+1})]$ and $[\ln(Y_{n-1}), \ln(Y_n), \ln(Y_{n+1})]$ for every $n \in [2, N-1] \subset \mathbb{N}$.

The corresponding results for local powers of $\delta_L(\mathrm{Ma})$, $\delta_R(\mathrm{Ma})$ and $\mathrm{Nu}(\mathrm{Ma})$ denoted γ_L, γ_R and γ_{Nu} respectively are presented in the figure 2.16. For a comprehensive comparison the exponents corresponding to the scaling laws for Nusselt number from numerical simulations, Hagstrom and Doering rigorous approach and piecewise SDP are also presented in the same figure.

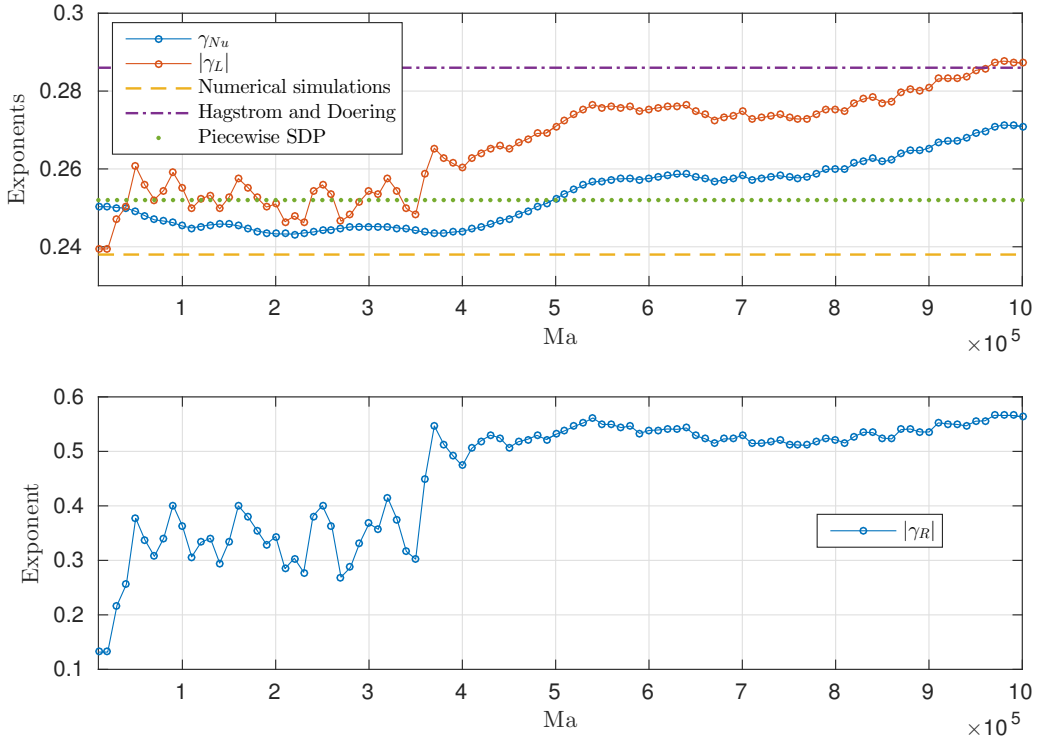

Figure 2.16: Scalings of an upper bound on Nusselt number and $\delta_L(\mathrm{Ma})$ (top) and $\delta_R(\mathrm{Ma})$ (bottom).

First of all, it can be clearly seen that the exponents for $\mathrm{Nu}(\mathrm{Ma})$ and $\delta_L(\mathrm{Ma})$ change synchronously which reinforces our suggestion that the scaling of Nusselt number is determined by the scaling of the left part of τ' profile. They oscillate around 0.245 and 0.253 respectively at Marangoni numbers $10^4 \leq \mathrm{Ma} \lesssim 3.5 \times 10^5$, but as $\mathrm{Ma} = 3.5 \times 10^5$ is passed, a continuous increase of γ_L and γ_{Nu} can be observed at each subsequent Marangoni number. We suspect that γ_{Nu} approaches the exponent $2/7$ corresponding to the Hagstrom and Doering rigorous upper bound. The similar behaviour can be seen for γ_R. It oscillates around 0.34 for $\mathrm{Ma} \lesssim 3.5 \times 10^5$ and suddenly jumps to approximately 0.54 for subsequent higher Marangoni numbers.

The explanation of this phenomenon can be easily obtained if we look at the ground state eigenvalues shown in the figure 2.17. As expected, a critical wavenumber $k = 3$ is present for all Marangoni numbers being considered. What is more interesting, the second critical wavenumber appears at $\mathrm{Ma} \approx 3.5 \times 10^5$ and, therefore, causes the significant change in γ_L, γ_R and γ_{Nu} which we see in the figure 2.16. In fact, the exponents oscillations would continue in a similar fashion if additional wavenumbers were merely not taken into consideration. Since high wavenumbers affect only the right part of τ' profile as we have already

shown in the previous sections, we can assert that the growth of γ_L and, consequently, γ_{Nu} is triggered by the jump in γ_R.

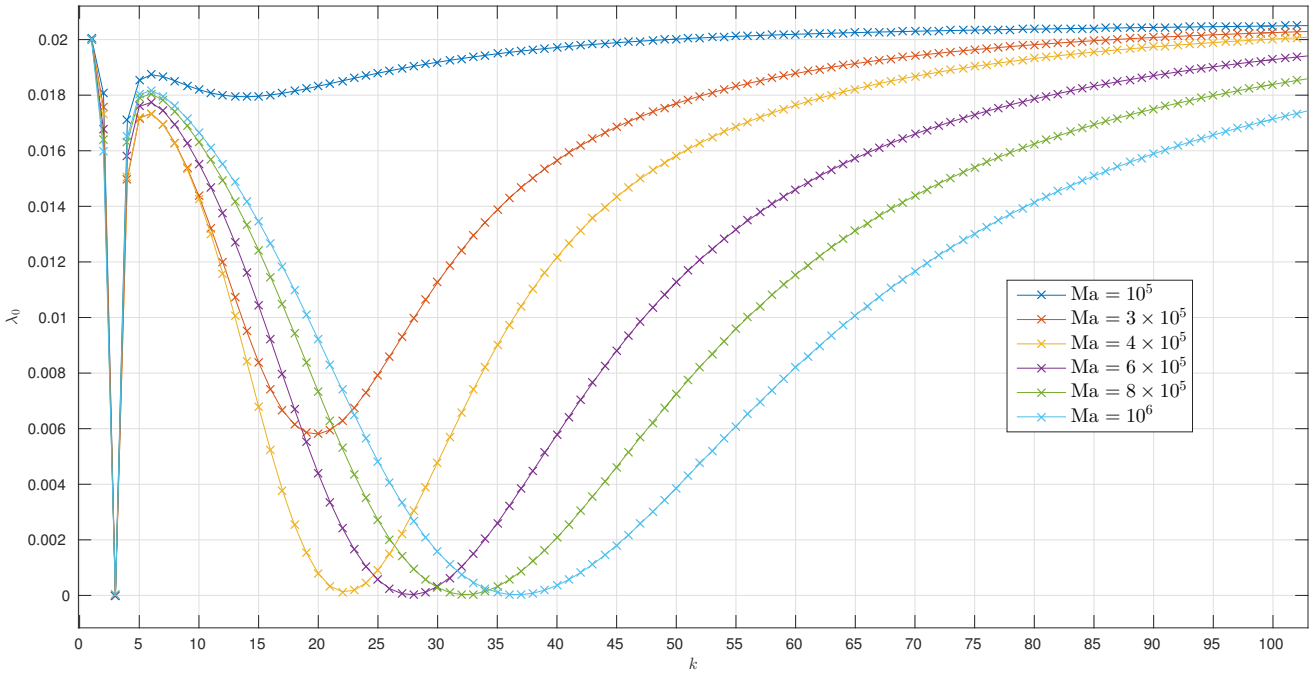

Figure 2.17: Ground state eigenvalues.

It can be also seen from the figure 2.17 that instead of a pair of higher critical wavenumbers we have the single second critical wavenumber. Moreover, it appears at much higher Marangoni numbers (Ma $\gtrsim 3.5 \times 10^5$) than in the piecewise SDP case (Ma $\gtrsim 5 \times 10^4$). Furthermore, it can be observed that as the second critical wavenumber is passed, all eigenvalues converge to some value (≈ 0.021) as k grows that resembles the picture we saw in the SDP case, but here the convergence is more clear and there is no evidence of the third critical wavenumber. The procedure of finding of the second critical wavenumber is the same as in the SDP case: we solve an optimization problem for a single wavenumber $k = 3$ and if there are negative ground state eigenvalues, we repeat calculations taking into consideration only the lowest minimum ground state eigenvalue which makes all other ground state eigenvalues positive.

2.7 Limitations of numerical solutions

As one can note from (2.27), k_{max} grows as $\mathrm{Ma}^{1/2}$ which means that even for Ma$= 4 \times 10^6$ we cannot be confident that our solution is feasible for all wavenumbers because we have to check k up to $k_{max} \approx 800$. However, $f_k(z)$ cannot be even accessed (in terms of Matlab functions) when $k \gtrsim 360$. In other words, important features of $f_k(z)$ are so tiny at high k that it is hard to represent numerically. Perhaps, it is

possible to rearrange terms in $f_k(z)$ and expand them in exponent functions or power series in a nested form that would not include arithmetic operations with both very small numbers close to machine epsilon and relatively large ones. This approach has not been employed, but it may allow to increase significantly available k.

However, we also observe that the optimal profiles in both numerical approaches are sensitive to the fine features of $f_k(z)$ and we thus want our solution to capture these features which means that we need to increase constantly the number of Legendre coefficients and the mesh density as Marangoni number increases because otherwise our solution is not reliable because a scaling law at very large Ma is extremely sensitive to the tiny features of τ'. It was observed that even for 200 Legendre coefficients a solution requires significant amount of time even for the modest number of wavenumbers being considered.

These issues together significantly limit our numerical capabilities because we always risk to fall into one of the following problems:

1. round-off errors of finite arithmetic;
2. impossibility to consider necessary $f_k(z)$;
3. getting result which is not feasible (if we ignore very high k);
4. extremely slow convergence to solution.

Analysis of self-similar parametrized profile

3.1 Qualitative understanding of optimization problem

Before proceeding into details, we shall reformulate the objective function in order to get more understanding of behaviour that we observe in numerics. If we apply a boundary condition $\tau(0) = 0$ to the (1.34), we obtain

$$\frac{1}{\mathrm{Nu}} \geq -\int_0^1 \left(\tau'^2 + 2\tau'\right) dz \tag{3.1}$$

and therefore completing the square and inversing the expression at both sides gives

$$\mathrm{Nu} \leq \frac{1}{1 - \int_0^1 (\tau' + 1)^2 \, dz} \tag{3.2}$$

provided that $\int_0^1 (\tau' + 1)^2 < 1$.

Thus, our objective is to minimize the expression on the right-hand side of the inequality (3.2) which is exactly the same as the requirement to minimize the value of the functional

$$I[\tau'] := \int_0^1 \left(\tau' + 1\right)^2 dz. \tag{3.3}$$

The stationary point of $I[\tau']$ is $\tau'(z) = -1$ for all z which gives the minimum possible bound $\mathrm{Nu} \leq 1$. However, we have to impose integral inequality constraints stated in (1.38) that eventually gives us a profile observed in the SDP results. As shown in the figure 2.7, at both sides of this profile the value of τ' is equal to -1. As we remember from the figure 2.9, $f_k(z) \approx 0$ near $z = 0$ and $z = 1$, so the sign-indefinite term in the integral inequality is negligible compared to the positive terms at the values of z close to $z = 0$ and $z = 1$. Therefore, we can argue that the constraint is not affected by τ' near $z = 0$ and $z = 1$ which finally gives $\tau'(0) = \tau'(1) = -1$ observed in the SDP results. In other words, τ' always tends to -1, but the integral constraint pushes it upward.

3.2 Parametrization of background profile

In the light of numerical results, it was proposed in [21] that the parametrization of background profile employing the property of self-similarity could be considered in order to capture the interaction between

two parts of profiles. Namely, the following form of parametrization was suggested

$$\tau'(z) = \begin{cases} f(z\mathrm{Ma}^{\delta}), & 0 \le z \le \mathrm{Ma}^{-\delta}, \\ 0, & \mathrm{Ma}^{-\delta} \le z \le 1 - \mathrm{Ma}^{-\gamma}, \\ g((1-z)\mathrm{Ma}^{\gamma}), & 1 - \mathrm{Ma}^{-\gamma} \le z \le 1. \end{cases} \tag{3.4}$$

Boundary conditions on $f(s)$ and $g(s)$ are deduced from our previous analysis of the objective function and numerical results. On the one hand, at $z = 0$ and $z = 1$ profile τ' must equal to -1 from the argument given in the previous section which gives a boundary condition $f(0) = g(0) = -1$. On the other hand, we saw in numerical results that the left and right parts of τ' tend to zero as z approaches the middle of profile. We therefore expect that a boundary condition $f(1) = g(1) = 0$ must be satisfied.

An important note must be taken about the structure of this parametrization. As it can be seen, both $f(z\mathrm{Ma}^{\delta})$ and $g((1-z)\mathrm{Ma}^{\gamma})$ are compressing as Ma increases assuming that δ and γ are positive. However, these functions does not scale in a vertical direction, i.e. $||f||_{\infty}$ and $||g||_{\infty}$ are constant and independent on Ma. Such a behaviour may be correct for the case of $g((1-z)\mathrm{Ma}^{\gamma})$ because we indeed observe a lack of steady scaling of the pick of the right part of τ' profile, but the left part's pick scales with respect to Marangoni number in a quite stable and predictable manner. At the moment, it is not obvious whether this property of τ' profile crucial or not, but we should bear in mind that it may affect the power laws being sought.

When the parametrized profile (3.4) was applied to the infinite-dimensional optimization profile (1.38), an upper bound on Nusselt number was expressed in the form of a scaling law

$$\mathrm{Nu} < \mathcal{O}\left(\mathrm{Ma}^{\min\{\delta,\gamma\}}\right). \tag{3.5}$$

It is also known from [21] that when the parametrized profile is applied to the full integral inequality as stated in (2.3), rearranging the integral terms and bounding the resulting integrals by Cauchy-Schwartz inequalities give a new algebraic inequality

$$-c_k \ge \frac{1}{2}\left(\mathrm{Ma}^{\frac{1-7\delta+\gamma}{2}} c_a + \mathrm{Ma}^{\frac{1-2\gamma}{2}} ||b_k||_{\infty}\right)^2 \tag{3.6}$$

where $c_a \in \mathbb{R}$ is a constant depending on the norm of $f(s)$ and already discussed approximation of $f_k(z)$ near $z = 0$ and b_k, c_k are defined as follows

$$b_k(t) = \int_{(1-t)\mathrm{Ma}^{\gamma}}^{1} g(s) f_k(1 - s\mathrm{Ma}^{-\gamma}) ds, \; 1 - \mathrm{Ma}^{-\gamma} \le t \le 1, \tag{3.7}$$

$$c_k = b_k(1) = \int_0^1 g(s) f_k(1 - s\mathrm{Ma}^{-\gamma}) ds. \tag{3.8}$$

Likewise the original integral constraint, the new inequality has to be satisfied for all $1 \le k < k_{max}$ where k_{max} is defined as in (2.27).

From the scaling law (3.5) we can observe that the lowest asymptotic upper bound on Nusselt number is obtained when either δ or γ are minimized subjected to (3.6). This leads to an optimization problem in the following form

$$\min_{\delta,\gamma} \; \min\{\delta, \gamma\} \tag{3.9}$$

$$\text{subject to } -c_k \ge \frac{1}{2}\left(\mathrm{Ma}^{\frac{1-7\delta+\gamma}{2}} c_a + \mathrm{Ma}^{\frac{1-2\gamma}{2}} ||b_k||_{\infty}\right)^2 \text{ for all } 1 \le k < 0.4\mathrm{Ma}^{1/2}. \tag{3.10}$$

In this chapter we concentrate our attention on this optimization problem without looking at the problem of satisfying condition $\mathrm{Nu} \geq 0$ which also arises in [21] and has to be eventually addressed.

3.3 Attempts to satisfy new inequality

Our purpose is to retrieve a dependence of c_k and $||b_k||_\infty$ on Marangoni number. Being done this, it is merely an algebraic and calculus task to determine appropriate constants to satisfy the inequality (3.6). Indeed, imagine that the following expressions correct for all large enough Ma and necessary k have been found

$$-c_k \geq \hat{c}\mathcal{O}(\mathrm{Ma}^m), \tag{3.11}$$

$$||b_k||_\infty \leq \hat{b}\mathcal{O}(\mathrm{Ma}^n). \tag{3.12}$$

Then, the inequality (3.6) becomes

$$\left(\frac{\mathrm{Ma}^{\frac{1-7\delta+\gamma}{2}}}{\mathcal{O}(\mathrm{Ma}^m)} \frac{c_a}{\hat{c}^{1/2}} + \frac{\mathrm{Ma}^{\frac{1-2\gamma}{2}}\mathcal{O}(\mathrm{Ma}^n)}{\mathcal{O}(\mathrm{Ma}^m)} \frac{\hat{b}}{\hat{c}^{1/2}} \right)^2 \leq 2 \tag{3.13}$$

and may be satisfied if δ and γ are found such that

$$\lim_{\mathrm{Ma}\to\infty} \frac{\mathrm{Ma}^{\frac{1-7\delta+\gamma}{2}}}{\mathcal{O}(\mathrm{Ma}^m)} \text{ is finite,} \tag{3.14}$$

$$\lim_{\mathrm{Ma}\to\infty} \frac{\mathrm{Ma}^{\frac{1-2\gamma}{2}}\mathcal{O}(\mathrm{Ma}^n)}{\mathcal{O}(\mathrm{Ma}^m)} \text{ is finite,} \tag{3.15}$$

which prevents blow-up of the left-hand side of the inequality. Constants c_a, $\hat{c}$, $\hat{b}$ depend on the norms of $f(s)$ and $g(s)$ and, thus, can be appropriately adjusted to make an algebraic inequality satisfied.

Before proceeding further and speculating about the form of $g(s)$, we should note that there is an inevitable condition on c_k coming directly from the inequality (3.6): c_k must be non-positive for all $k \leq k_{max}$ and for all large enough Ma. As $f_k(1 - s\mathrm{Ma}^{-\gamma})$ is known to be non-positive for any $k, \mathrm{Ma}, \gamma \geq 0$ on $s \in [0, 1]$, this condition implies that $g(s)$ must be positive at least for some $s \in [0, 1]$. However, we have a boundary condition $g(0) = -1$ that immediately gives a conclusion that $g(s)$ must change sign at least once. Exactly this behaviour of $g(s)$ can be observed from the piecewise SDP results: the right part of τ' profile is mainly positive, but as $z \to 1$, τ' becomes negative and finally reaches $\tau'(1) = -1$. Hence, we can reasonably assume that there is only one point $s_{cr} \in [0, 1]$ where $g(s)$ changes its sign such that

$$g(s) < 0 \text{ if } s \in [0, s_{cr}], \tag{3.16}$$

$$g(s) \geq 0 \text{ if } s \in (s_{cr}, 1]. \tag{3.17}$$

However, such a general case of $g(s)$ is quite difficult to consider because of the norm $||b_k||_\infty$. Moreover, there is a hidden problem in c_k when sign-indefinite $g(s)$ is used. To show it, divide the integral (3.8) into positive and negative parts:

$$c_k = \int_0^{s_{cr}} g(s) f_k(1 - s\mathrm{Ma}^{-\gamma}) ds + \int_{s_{cr}}^1 g(s) f_k(1 - s\mathrm{Ma}^{-\gamma}) ds. \tag{3.18}$$

Since $f_k(1-s\mathrm{Ma}^{-\gamma})$ concentrates near $s=0$ as k increases, it can be roughly said that for any $s_f \in [0,1]$ we can find such k that $f_k(1-s\mathrm{Ma}^{-\gamma}) \approx 0$ for all $s > s_f$. Therefore, it is always possible to find such k_{cr} that the second integral in (3.18) will be negligible compared to the first one. Hence, only the positive part of c_k remains which means that $-c_k$ will be negative for all $k > k_{cr}$ and (3.6) cannot be satisfied. It means that one has to take only such $g(s)$ that $k_{max} < k_{cr}$.

In contrast, a positive $g(s)$ is much easier to treat because in this case $||b_k||_\infty = c_k$ and the problem described above automatically disappears. We will consider this form of $g(s)$ expressed as $g(s) = G$ where G is some positive constant assuming that the boundary layer $[0, s_{cr}]$ is infinitesimally small, i.e. $s_{cr} \to 0$, which allows to satisfy the boundary condition. One can note that this form of the right part is the same as in the discontinuous optimization.

Then, c_k becomes an integral of f_k

$$c_k = G\int_0^1 f_k(1-s\mathrm{Ma}^{-\gamma})ds \tag{3.19}$$

and recalling that $||b_k||_\infty = c_k$ for this choice of $g(s)$, the inequality (3.6) transforms to

$$\left(\frac{\mathrm{Ma}^{\frac{1-7\delta+\gamma}{2}}}{|c_k|^{1/2}}\frac{c_a}{G^{1/2}} + \mathrm{Ma}^{\frac{1-2\gamma}{2}}|c_k|^{1/2}G^{1/2}\right)^2 \le 2. \tag{3.20}$$

It is now essential to consider the behaviour of $|c_k|$ for a range of k. For k close to $k \approx \mathrm{Ma}^\gamma$ a function $f_k(1-s\mathrm{Ma}^{-\gamma})$ can be quite precisely approximated by fourth-order Taylor expansion about $s=0$:

$$f_k(1-s\mathrm{Ma}^{-\gamma}) = -H_1(k)k\mathrm{Ma}^{-\gamma}s + \frac{1}{2}k^2\mathrm{Ma}^{-2\gamma} - \frac{1}{6}H_3(k)k^3\mathrm{Ma}^{-3\gamma} + \frac{1}{12}k^4\mathrm{Ma}^{-4\gamma} + \mathcal{O}(s^5) \tag{3.21}$$

where $H_1(k) := \frac{\sinh^2(k)-k^2}{\sinh(2k)-2k}$ and $H_3(k) := \frac{3\cosh(k)^2 2-3-k^2}{\sinh(2k)-2k}$ are virtually independent on k when high k are considered, so they are taken to be constant in the current context. Considering for convenience $k = \mathrm{Ma}^m$ we can rewrite it as

$$f_k(1-s\mathrm{Ma}^{-\gamma}) \approx -H_1(k)\mathrm{Ma}^{m-\gamma}s + \frac{1}{2}\mathrm{Ma}^{2(m-\gamma)}s^2 - \frac{1}{6}H_3(k)\mathrm{Ma}^{3(m-\gamma)}s^3 + \frac{1}{12}\mathrm{Ma}^{4(m-\gamma)}s^4 \tag{3.22}$$

and immediately see that for $m=\gamma$ the function $f_k(1-s\mathrm{Ma}^{-\gamma})$ and, consequently, $|c_k|$ do not depend on Ma, so $|c_k| = \text{const}$ at $k = \mathrm{Ma}^\gamma$. Moreover, it can be shown by ordinary calculus that $\max_m |c_k|$ also happens when $m \approx \gamma$ which leads us to an important result that $\sup_k |c_k| = |c_k|_{k\approx\mathrm{Ma}^\gamma} = C$ where C is independent on Ma. Therefore, we modify the inequality (3.20):

$$\left(\frac{\mathrm{Ma}^{\frac{1-7\delta+\gamma}{2}}}{|c_k|^{1/2}}\frac{c_a}{G^{1/2}} + \mathrm{Ma}^{\frac{1-2\gamma}{2}}C^{1/2}G^{1/2}\right)^2 \le 2. \tag{3.23}$$

On the other hand, for low k the function $f_k(1-s\mathrm{Ma}^{-\gamma})$ behaves linearly and, therefore, can be approximated by merely first-order Taylor expansion

$$f_k(1-s\mathrm{Ma}^{-\gamma}) = -H_1(k)\mathrm{Ma}^{m-\gamma}s + \mathcal{O}(s^2) \tag{3.24}$$

and then

$$|c_k| \approx \mathrm{Ma}^{m-\gamma}. \tag{3.25}$$

Substituting it into inequality gives

$$\left(\mathrm{Ma}^{\frac{1-7\delta+2\gamma-m}{2}} \frac{c_a}{G^{1/2}} + \mathrm{Ma}^{\frac{1-2\gamma}{2}} C^{1/2} G^{1/2}\right)^2 \leq 2. \tag{3.26}$$

As this inequality has to be satisfied for all k up to $k_{max} \propto \mathrm{Ma}^{1/2}$, the following optimal values of δ and γ are obtained

$$\delta = \frac{2}{7}, \tag{3.27}$$

$$\gamma = \frac{1}{2}. \tag{3.28}$$

Since $\mathrm{Nu} < \mathcal{O}\left(\mathrm{Ma}^{\min\{\delta,\gamma\}}\right)$, Nusselt number thus scales as $\mathrm{Nu} \propto \mathrm{Ma}^{2/7}$ which exactly coincides with the power law of Hagstrom and Doering. The main problem seems to be the fact that $\sup_k |c_k|$ does not scale with respect to Marangoni number for a necessary range of wavenumbers which forces us to set $\gamma = 1/2$. This result immediately leads to $\delta = 2/7$ because of the linear behaviour of $f_k(1 - s\mathrm{Ma}^{-\gamma})$ for small k that a priori have to be taken into account. Non-constant positive $g(s)$ will not change this behaviour because the dependence on Ma is localized in $f_k(1 - s\mathrm{Ma}^{-\gamma})$.

This analytical result is supported by the numerical results obtained using discontinuous piecewise optimization. The same profile has been investigated there and we indeed observed that when the second critical wavenumber appears at $\mathrm{Ma} \approx 3.5 \times 10^5$ the scaling of the right part of profile suddenly becomes $\gamma \approx 1/2$ and synchronically the scaling of the left part starts converging to $\delta \approx 2/7$.

Discussion and conclusions

4.1 Improvement of parametrized profile

In the previous chapter we have considered the simplest case of $g(s)$, namely, when it is positive at $s \in [0, 1]$. However, using positive $g(s)$ we neglect a negative part of the right boundary layer assuming that it is too small to be considered. Comparison of the SDP results and discontinuous optimization results along the analysis of the positive $g(s)$ shows that the negative boundary layer may play a significant role in the power law for an upper bound on Nusselt number. Considering a function $g(s)$ having positive and negative parts assumes that $||b_k||_\infty \neq |c_k|$ and, therefore, recalling that $c_k = b_k(1)$ the inequality (3.6) can be rewritten in the following form

$$\left(\mathrm{Ma}^{\frac{1-7\delta+\gamma}{2}} \frac{c_a}{b_k(1)^{1/2}} + \mathrm{Ma}^{\frac{1-2\gamma}{2}} \frac{||b_k||_\infty}{b_k(1)^{1/2}}\right)^2 \leq 2 \tag{4.1}$$

where $b_k(1)$ has to be negative.

One could try to analyse the behaviour of the quantity $\frac{||b_k||_\infty}{b_k(1)^{1/2}}$ which in general should scale with respect to Marangoni number even for wavenumbers of order $k \propto \mathrm{Ma}^\gamma$ that appeared to be crucial in the case of positive $g(s)$. If so, it will allow to make optimal γ smaller than $1/2$ which should result in a smaller δ and, consequently, a better scaling law for Nusselt number.

Another important aspect which is not addressed by the given form of the parametrized profile is a vertical scaling of $f(s)$. It can be clearly seen from τ' profiles obtained via the SDP that the pick of the left part of profile grows steadily as Marangoni number increases. Even though the positive part of it looks negligible compared to the large negative part, it becomes sufficiently large when Marangoni number reaches the value of 10^6 and, thus, may start playing an essential role at subsequent Marangoni numbers.

4.2 Improved upper bound for critical wavenumbers

Critical wavenumbers observed in both numerical studies are significantly lower than ones estimated by (2.27). For example, we saw in the analysis of the SDP results that the second critical wavenumber scales with respect to Marangoni number as $k_{cr} \propto \mathrm{Ma}^{1/10}$. Similar scaling was observed in the discontinuous piecewise optimization, whereas the analytically estimated maximum critical wavenumber scales as $k_{max} \propto \mathrm{Ma}^{1/2}$. This dramatic difference forces us to include into the analytical analysis wavenumbers that worsen the resultant scaling law. If it was possible to consider k up to $k_{cr} \propto \mathrm{Ma}^{1/10}$, then the problem with constant $\sup_k |c_k|$ might disappear. Since $|c_k|$ scales as $|c_k| \propto \mathrm{Ma}^{-\gamma}$ at low wavenumbers, it would allow to find an optimal scaling for the right part of profile $\gamma = 1/3$ which automatically yields a desirable scaling

for the left part and at the same time for Nusselt number $\delta = 5/21$. This result looks very optimistic because it almost exactly coincides with the power law (1.2) observed from the simulations of Boeck and Thess in [10].

4.3 Variational approach

There is an inevitable problem inherent in the approach considered in [21]. At some point of derivation it is necessary to use Cauchy-Schwartz bounds on integrals in order to transform the integral spectral constraint to the algebraic inequality (3.6). Since the left part of τ' profile is negative, whereas the right part of τ' is presumably mainly positive, it might be the case that when Cauchy-Schwartz bounds are imposed on integrals involving $f(s)$ and $g(s)$, an interplay between them is lost. In [21] some kind of such an interaction between these parts is preserved via the interaction between powers δ and γ and manifests itself in the first term in the inequality (3.6). However, there is no guarantee that this interaction is sufficient for deriving a better power law.

The common approach for infinite-dimensional optimization problems is a variational technique where Euler-Lagrange equations are derived for a corresponding problem. As it was discussed in the first section, a background profile $\tau'(z)$ can be in fact redefined as a function with fixed endpoints: $\tau'(0) = \tau'(1) = -1$. Then, the Fréchet derivative of the objective functional $\mathcal{B}[\tau']$ in (1.38) with respect to τ' can be easily calculated (in this context τ' is treated as merely a function). It is also necessary to take into consideration the constraints which is usually done by Lagrange multipliers. Euler-Lagrange equations for $Q_{\tau,k}[u]$ may produce eigenvalue problems for the underlying linear operators and we could require their ground state eigenvalues to be zero by means of Lagrange multipliers.

Unfortunately, there are two issues in this approach. First of all, it is not clear how to do it for the constraints $Q_{\tau,k}[u]$ because of the presence of $u(1)$ in (2.3). One could eliminate it by applying a substitution $\phi := uu(1)$ which leads to a modified integral inequality

$$Q_{\tau,k}[\phi] = \int_0^1 \left[\phi'^2 + k^2\phi^2 - 2\mathrm{Ma}\tau' f_k(z)\phi\right] dz \geq 0 \tag{4.2}$$

but in this case $Q_{\tau,k}[\phi]$ is no longer in the quadratic form. The second issue is related to the fact that we cannot impose the requirement for ground state eigenvalues of $Q_{\tau,k}[u]$ to be zero for all k because almost all of them in fact must be merely positive.

However, an additional insight into the problem may be gained if we consider every constraint $Q_{\tau,k}[\phi] \geq 0$ as a separate variational problem. One could minimize $Q_{\tau,k}[\phi]$ and obtain and expression for $\phi_{min}[\tau']$ which is again a functional. Substituting it back into $Q_{\tau,k}[\phi]$, we obtain a functional $Q_k[\tau]$ which is subjected to be non-negative and can be analysed for different background profiles.

Since ϕ has fixed endpoints $\phi(0) = 0$, $\phi(1) = 1$, the Euler-Lagrange equation for minimizing $Q_{\tau,k}[\phi]$ is

$$\phi'' - k^2\phi = \mathrm{Ma}\tau' f_k. \tag{4.3}$$

One may consult [14] where the variational machinery is demonstrated for a similar problem.

4.4 Does a better scaling law exist?

This work is concluded by a simple question: is it possible to obtain a better scaling law for an upper bound on Nusselt number from the variational problem (1.38) stated in the introduction?

Despite the fact that an additional understanding of the problem of power laws for Nusselt number has been acquired during this work, it is still far from obvious whether it is possible to prove analytically an existence of better scaling or not. Our attempts to simplify the form of the background profile τ' at the present time lead to the results coinciding with the rigorous upper bound of Hagstrom and Doering. The results of the full piecewise semidefinite optimization are more optimistic and produce the power law $\mathrm{Nu} \propto \mathcal{O}(\mathrm{Ma}^{0.252})$ for a range of Marangoni number from Ma^4 to Ma^6 where the exponent is significantly better than $2/7$. However, the existing numerical limitations do not allow to consider higher Marangoni numbers as well as higher wavenumbers. As one could notice, the pair of additional critical wavenumbers appears "out of the clear blue sky" and, even though we did not see any evidence, it is still not guaranteed that the fourth wavenumber of order $k \propto \mathcal{O}(10^3)$ does not exist for, say, $\mathrm{Ma} = 10^7$. Such an additional critical wavenumber may trigger an exponent of the corresponding power law to jump to $2/7$ as it happens in the discontinuous piecewise optimization.

On the other hand, assuming that the thinking above is incorrect and the power law will persist for higher Marangoni numbers and presumably higher-order critical wavenumbers, we can consider the numerical results from the semidefinite optimization as quite reliable, because even though they may be inaccurate, any improvement of accuracy (increasing the number of Legendre coefficients, refining the mesh, etc.) will probably only refine the accuracy of the exponent and pre-factor, but not change the power law dramatically. Therefore, there must be a way to prove an existence of a better scaling for an upper bound on Nusselt number.

To motivate future researches, one optimistic point should be added. The optimal background profile τ shown in the figure 2.6 is qualitatively exactly the same as a horizontally and time-averaged temperature profile obtained in the numerical simulations of Boeck and Thess (figure 2 in [10]). It can be noted from their work that all minor features of the temperature profile disappear as Marangoni number increases above $\mathrm{Ma} = 10^5$ leaving only distinctive features of the left and right boundary layers which were discussed in detail in the present work. Therefore, the variational problem (1.38) formulated by means the background profile method produces the profiles τ such that they seem to capture all important physical features of the underlying flow. As a result, we may expect that the minimization of an upper bound on Nusselt number may indeed produce the scaling law for Nusselt number.

References

[1] Lord Rayleigh O.M. F.R.S. On convection currents in a horizontal layer of fluid, when the higher temperature is on the under side. *Philosophical Magazine Series 6*, 32(192):529–546, 1916.

[2] E. Koschmieder. *Bénard cells and Taylor vortices (Cambridge monographs on mechanics and applied mathematics)*. Cambridge: Cambridge University Press, 1993.

[3] M. J. Block. Surface tension as the cause of Bénard cells and surface deformation in a liquid film. *Nature*, 168:650–651, 1956.

[4] J. R. A. Pearson. On convection cells induced by surface tension. *Journal of Fluid Mechanics*, 4:489–500, 1958.

[5] J. A. Maroto, V. Perez-Munuzuri, and M. S. Romero-Cano. Introductory analysis of Bénard-Marangoni convection. *European Journal of Physics*, 28(2):311, 2007.

[6] A. Kumar and S. Roy. Effect of three-dimensional melt pool convection on process characteristics during laser cladding. *Computational Materials Science*, 46(2):495 – 506, 2009.

[7] M. F. Schatz and G. P. Neitzel. Experiments on thermocapillary instabilities. *Annual Review of Fluid Mechanics*, 33(1):93–127, 2001.

[8] S. G. Yiantsios, S. K. Serpetsi, F. Doumenc, and B. Guerrier. Surface deformation and film corrugation during drying of polymer solutions induced by Marangoni phenomena. *International Journal of Heat and Mass Transfer*, 89:1083 – 1094, 2015.

[9] G. Hagstrom and C. R. Doering. Bounds on heat transport in Bénard-Marangoni convection. *Phys. Rev. E*, 81:047301, 2010.

[10] T. Boeck and A. Thess. Power-law scaling in Bénard-Marangoni convection at large Prandtl numbers. *Phys. Rev. E*, 64:027303, 2001.

[11] A. Pumir and L. Blumenfeld. Heat transport in a liquid layer locally heated on its free surface. *Phys. Rev. E*, 54:R4528–R4531, 1996.

[12] C. R. Doering and P. Constantin. Energy dissipation in shear driven turbulence. *Phys. Rev. Lett.*, 69:1648–1651, 1992.

[13] C. R. Doering and P. Constantin. Variational bounds on energy dissipation in incompressible flows: Shear flow. *Phys. Rev. E*, 49:4087–4099, 1994.

[14] C. R. Doering and P. Constantin. Variational bounds on energy dissipation in incompressible flows. III. Convection. *Phys. Rev. E*, 53:5957–5981, 1996.

[15] C. R. Doering, F. Otto, and M. G. Reznikoff. Bounds on vertical heat transport for infinite-Prandtl-number Rayleigh-Bénard convection. *Journal of Fluid Mechanics*, 560, 2006.

[16] J. P. Whitehead and R. W. Wittenberg. A rigorous bound on the vertical transport of heat in Rayleigh-Bénard convection at infinite Prandtl number with mixed thermal boundary conditions. *Journal of Mathematical Physics*, 55(9), 2014.

[17] S. Boyd and L. Vandenberghe. *Convex Optimization*. Cambridge University Press, New York, NY, USA, 2004.

[18] J. Löfberg. YALMIP : A toolbox for modeling and optimization in MATLAB. In *In Proceedings of the CACSD Conference, Taipei, Taiwan*, 2004.

[19] Yu. E. Nesterov and M. J. Todd. Self-scaled barriers and interior-point methods for convex programming. *Mathematics of Operations Research*, 22(1):1–42, 1997.

[20] G. Fantuzzi and A. Wynn. Optimal bounds with semidefinite programming: An application to stress-driven shear flows. *Phys. Rev. E*, 93:043308, 2016.

[21] A. Wynn. Personal correspondence, 2016.

[22] G. Fantuzzi, A. Wynn, P. Goulart, and A. Papachristodoulou. Optimization with affine homogeneous quadratic integral inequality constraints. 2016.